N72-23791

A NUMERICAL SOLUTION OF THE NAVIER-STOKES EQUATIONS FOR SUPERCRITICAL FLUID THERMODYNAMIC ANALYSIS

P. J. Heinmiller
TRW Systems Group
Houston, Texas

May 1971

ABSTRACT

An explicit numerical solution of the compressible Navier-Stokes equations is applied to the thermodynamic analysis of supercritical oxygen in the Apollo cryogenic storage system. The wave character is retained in the conservation equations which are written in the basic fluid variables for a two-dimensional Cartesian coordinate system. Control-volume cells are employed to simplify imposition of boundary conditions and to ensure strict observance of local and global conservation principles. Non-linear real-gas thermodynamic properties responsible for the pressure collapse phenomonon in supercritical fluids are represented by tabular and empirical functions relating pressure and temperature to density and internal energy. Wall boundary conditions are adjusted at one cell face to emit a prescribed mass flowrate. Electrical heater input is treated as localized internal heat generation, a fraction of which may be radiated to the walls where it is added to the prescribed boundary heat flux. The effect of "tank stretch" on dP/dt is included as out-of-plane fluid expansion. Scaling principles are invoked to achieve acceptable computer execution times for very low Mach number convection problems. Detailed simulations of thermal stratification and fluid mixing occurring under low acceleration in the Apollo 12 supercritical oxygen tank are presented which model the pressure decay associated with de-stratification induced by an ordinary vehicle maneuver and heater cycle operation.

ACKNOWLEDGMENT

The author wishes to express his appreciation to Dr. W. E. Simon of NASA-MSC who contributed a number of helpful suggestions and provided the necessary computing support.

TABLE OF CONTENTS

INTRODUCTION

Origin of Problem

Gaseous oxygen required for life-support and electrical power generation aboard the Apollo Command and Service Module is stored in super-insulated double-wall spherical tanks which are a portion of the storage and supply system. In these tanks, oxygen is maintained at cryogenic temperatures and at pressures somewhat above the critical pressure. (See Table 1 for system operating parameters.) Under these conditions, the oxygen is in the super-critical state which results in a high-density single-phase compressible fluid suitable for expulsion under zero-gravity conditions.

Storage tank pressure is maintained relatively constant during fluid withdrawal by increasing the fluid temperature using an internal filament-type electrical heater. Prior to and including Apollo 13, the energy supplied by this heater was dispersed throughout the fluid by means of internal mixing fans. However, following the failure of the oxygen system during the Apollo 13 mission, the mixing fans were removed from subsequent oxygen tanks to minimize the possible combustion hazard.

Numerical studies by Kamat and Abraham [2] have shown that a substantial decrease in pressure can result from fluid mixing if the heater input is not well distributed beforehand. The decrease in pressure can be of sufficient magnitude to cause the fluid to return to a two-phase condition. Since natural convection would have to be relied upon to limit the temperature concentrations, a considerable effort was initiated to refine the understanding of the thermodynamic and fluid dynamic behavior of locally-heated supercritical oxygen stored in a low acceleration environment.

Stratification and Pressure Collapse

Due to the low thermal conductivity of supercritical oxygen, electricial heaters generate local heat concentrations. Under low accelerations, these concentrations do not disperse rapidly. Without a mechanical means of mixing the heated fluid with the surrounding cold fluid, subsequent heater cycles result in increasingly severe heat concentrations, or "thermal stratification."

Thermophysical properties of oxygen in the vicinity of the critical point are strongly nonlinear and therefore deviate from the properties of an ideal gas. One of the ramifications of the specific heat

nonlinearity is that the bulk fluid temperature is not equal to the equilibrium temperature which would exist if the fluid were mixed or otherwise brought to thermal equilibrium.

The equation of state is also nonlinear in this region and is sensitive to small changes in temperature. The result is that a modest drop in the bulk temperature brought about by fluid mixing from a stratified condition can cause a substantial decrease in pressure or "pressure collapse". Kamat and Abraham [2] have shown that the pressure decreases monotonically with mixing so that the final pressure is always below any intermediate pressure. It is possible for the collapse pressure to drop below the critical pressure in which case the fluid becomes sub-critical, a condition in which liquid and gaseous phases may co-exist. This condition must be avoided if a uniform single phase fluid expulsion is to be maintained.

This paper describes an explicit numerical solution of the compressible conservation equations that govern natural convection in compressible fluids. Real fluid thermodynamic relations are employed so that the pressure collapse phenomenon can be observed in super-critical fluids. A number of additional effects have been incorporated in the solution for engineering application including "tank stretch," heater thermal mass, and heater radiation.

Comparisons are made between the results of the present solution and Apollo 12 flight data occurring at 8 hours GET. Several other verification test cases also are presented to demonstrate the program capability.

Table 1 Cryogenic System Operational Parameters* - Oxygen

(Apollo 14 And Subsequent)

Stored Fluid Weight (100% indication)	330.1 lb
Usable Fluid Weight	323.5 lb
Tank Volume	4.75 ft^3
Normal Operating Pressure	900 $\pm$ 35 psi
Pressure Switch Deadband (Min)	30 psi
Total Heater Power (prior to Apollo 14)	434.8 B/hr (528.6)
Bulk Fluid Temperature	160 to 530 °R

* Data taken from Reference 1

APPROACH

Under low acceleration conditions, the potential pressure collapse depends primarily upon the amount of heat concentrated in the portion of fluid surrounding the heater. The heater cycle time, however, depends upon the actual pressure rise and decay rates which, in turn, are related to the processes taking place in the heater thermal boundary layer and to other effects such as tank stretch. At 95% of tank quantity, tank stretch decreases the magnitude of the pressure rate and therefore the cycle time by almost a factor of two[1].

A detailed knowledge of the temperature, density, and fluid velocity distributions is necessary in order to describe the heating and mixing processes and the resulting thermodynamic behavior of supercritical oxygen in the Apollo cryogenic storage tanks. This information can be obtained only by simultaneously solving the conservation equations of mass, momentum, and energy. These equations are coupled nonlinear partial differential equations which are not amenable to analytical solutions for any but the most restrictive of problems. However, finite-difference numerical techniques have been developed which allow these equations to be solved in their entirety.

The general solution procedure is to integrate numerically the conservation equations from a given set of initial conditions subject to the various boundary conditions imposed by the physical system. Although the fluid motion in the Apollo storage tanks is three-dimensional, a two-dimensional solution of the conservation equations is adequate to resolve the basic mechanisms which produce stratification and mixing.

The basic model consists of a two-dimensional fluid slab of unit depth to which the conservation equations are applied. The momentum equations include the gravitational body force terms so that natural convection may develop. The basic provisions necessary to model the Apollo storage tank are: two acceleration components, a localized internal heat source, external heat leak, and a fluid outlet port. Non-linear thermodynamics require that real-gas properties be used. To adequately describe the actual pressure rise rate for engineering purposes, a number of refinements to the idealized model were required which include accounting for the thermal mass of the heater, heater radiation to the tank wall, and tank stretch.

Acceleration Components

In general, two acceleration components are required to describe the body forces acting on the fluid. Stratification develops under a

uniform low-level acceleration in a constant relative direction. Such an acceleration arises from the centripetal acceleration $(\vec{\omega} \times \vec{\omega} \times \vec{r})$ associated with the three revolutions per hour roll rate used for passive thermal control (PTC).

Maximum mixing resulting from a G-spike, (e.g., RCS thruster firing) occurs when the direction of the G-spike is normal to the density gradient. A tangential acceleration $(\dot{\vec{\omega}} \times \vec{r})$ results from a change in the roll rate during spin-up to or de-spin from the PTC mode. The effects of coriolis acceleration, non-constant radius vector, and planetary gravity gradient are insignificant compared to the acceleration forces discussed above and are not considered in this analysis.

Internal Heater

The heater element is simulated as an internal energy source at an appropriate location in the fluid volume. No velocity boundary conditions are attempted at these "heater cells" due to the computational difficulty in resolving the flow boundary layer. The heater does not represent the heater cylinder itself but rather the heated fluid sheath surrounding the heater cylinder. The number of heater cells is selected such that the combined volume is equal to the "effective boundary layer volume". This effective volume has been postulated in order to explain observed pressure rise rates, since the grid spacing of the numerical solution is too coarse to resolve the actual thermal boundary layer. The effective boundary layer volume was derived on the basis of empirical flight data.

Heater Thermal Mass Effect

Heater-on operation is modeled as a prescribed heat generation rate within the heater cells. When steady-state heating conditions are approached, a power balance at the heater implies that the impressed electrical power is converted directly to a heating rate of the fluid sheath surrounding the heater. The heater thermal mass absorbs heater power until heat conduction into the fluid reaches steady-state. For the present purposes, this build-up rate is approximated as an equivalent linear ramp up to the steady-state rate which occurs during the interval T_{lag}. (See Nomenclature.) Defining C_{lag} as a ramp function, the internal heat generation rate then is given by:

$$\dot{Q} = C_{lag} \dot{Q}_{heater} \qquad (1)$$

After the heater is turned off, the heater cylinder rejects the heat stored in its thermal mass. Assuming that the heater temperature returns to the previous low temperature, the inverse linear ramp was used for flux decay. The internal heat generation rate during the heater-off ramp then becomes

$$\dot{Q} = (1 - C_{lag})\ \dot{Q}_{heater} \tag{2}$$

Heater Radiation

During the latter portions of the Apollo mission, the heater temperature rises high enough that thermal radiation plays an important heat transfer role. At a specified time in the mission, the energy radiated from the heater may be represented as a constant fraction of the heater power not absorbed by the thermal mass:

$$\dot{Q}_{rad} = C_{rad}\ (C_{lag}\ \dot{Q}_{heater}) \tag{3}$$

and the rate of heat entering the fluid becomes:

$$\dot{Q} = (1 - C_{rad})\ C_{lag}\ \dot{Q}_{heater} \tag{4}$$

Outlet Port

A fluid outlet port is modeled at the periphery of the fluid volume by specifying a fluid velocity at a location on the boundary such that the prescribed mass withdrawal rate occurs. This same velocity is used to convect momentum and energy from the system.

It was necessary to relocate the outlet port from its actual position to a position lying in the plane of the model. The flow distortion introduced by this relocation appears to be negligible for the flowrates presently being considered.

Heat Leak

Heat entering the fluid after passing through the super-insulation surrounding the storage tank is called heat leak and for the Apollo oxygen tank has a nominal value of about 25 BTU/hr. The quantity entering the fluid model is proportioned according to the volume ratio C_{vol}. Heat leak is imposed as a uniformly distributed heat flux over the exposed fluid boundary. The decision to specify the heat flux at the

boundary as opposed to specifying the boundary temperature was based upon the fact that the rate of heat leak into the fluid is more accurately known than the wall temperature of the inner tank. Global conservation principles also are more easily satisfied. Since oxygen is primarily transparent in the region, the energy radiated from the heater cylinder is not absorbed until it reaches the tank wall from which it enters the fluid by conduction.

Tank Stretch/Line Compression

The elasticity of the thin-wall tank permits a volume expansion with pressure (dV/dP) of about 3.6×10^{-5} ft^3/psi at the normal operating pressure. At high tank quantities (80%-100%) fluid pressure is very sensitive to density, and variations in tank volume have a significant effect on the pressure rise rate [1, p3-16] decreasing the magnitude of dP/dt by over 40% at 95% quantity. Tank stretch is modeled as an out-of-plane fluid expansion by permitting the unit z dimension to vary with pressure according to dV/dP.

Seto[3] derived an expression for the effect on dP/dt of fluid compression in the external plumbing. Tests with the equilibrium tank model described in this reference show that this effect is of the same order as the effect of tank stretch. For the present purpose, line compression is represented as an increase in the tank stretch factor dV/dP.

GOVERNING EQUATIONS

General Discussion

The equations governing the conservation of mass, momentum, and energy in a fluid system may be formulated in either Eulerian or Lagrangian coordinates. The Lagrangian formulation fixes the coordinate system in the fluid mass and is convenient for problems involving a free surface. However, accuracy is seriously impared with time as the coordinates deform and move with fluid convection.[4] In the Eulerian formulation, the coordinate system is fixed in the fluid volume so that the fluid moves through the coordinate system. For this reason, the Eulerian formulation is generally superior for complex convection problems and is used for the present analysis.

Richtmyer and Morton [4] and others recommend the use of conservation equations in the "conservative" or "divergence" form which preserves the conservation principles when solved at a finite number of discrete points. If the conservative form is not used, computational sources and sinks can appear as fluid is convected from one cell to the next, their origin being the non-constant coefficients appearing in front of the derivatives. For example, the mass leaving a cell through one of its faces does not necessarily appear in total in the adjacent cell. Although these errors are small, they occur at each cell interface at each time step and can accumulate with time. The propagation of these errors eventually can lead to computational instability. Computationally non-conservative equations are derived by performing flux balances on an infinitesimal control volume[5]. These equations can be converted to conservative form by adding the continuity equation to each of the other three conservation equations. The divergence form is developed directly from surface and volume integrals of flux vectors employing the Gauss Divergence Theorem[6].

A very clean form of the general conservation equations was obtained with minor modification from Goodrich[7]. These equations are in conservative form and are written in terms of the basic fluid variables for a two-dimensional Cartesian coordinate system. The non-dimensional form was not used because of the difficulty in assigning characteristic reference values for non-linear real fluid thermodynamic properties.

The general equations governing a compressible viscous fluid with body forces and internal heat source are:

Mass Continuity

$$\frac{\partial \rho}{\partial t} + \frac{\partial (\rho u)}{\partial x} + \frac{\partial (\rho v)}{\partial y} = 0 \tag{5}$$

X-Component Momentum

$$\frac{\partial (\rho u)}{\partial t} + \frac{\partial}{\partial x}(\rho uu + P + \tau_{xx}) + \frac{\partial}{\partial y}(\rho uv + \tau_{xy}) = \rho g_x \tag{6}$$

Y-Component Momentum

$$\frac{\partial (\rho v)}{\partial t} + \frac{\partial}{\partial x}(\rho vu + \tau_{xy}) + \frac{\partial}{\partial y}(\rho vv + P + \tau_{yy}) = \rho g_y \tag{7}$$

Energy

$$\frac{\partial (\rho E)}{\partial t} + \frac{\partial}{\partial x}[(\rho E + P)u + q_x + u\tau_{xx} + v\tau_{xy}] + \frac{\partial}{\partial y}[(\rho E + P)v + q_y + v\tau_{yy} + u\tau_{xy}] = \dot{Q}_v \tag{8}$$

where:

$$E = e + \tfrac{1}{2}(u^2 + v^2) \tag{9}$$

$$P = P(\rho, e) \tag{10}$$

$$T = T(\rho, e) \tag{11}$$

$$q_x = -k \frac{\partial T}{\partial x} \qquad q_y = -k \frac{\partial T}{\partial y} \tag{12}$$

$$\tau_{xx} = -\frac{2}{3}\mu\left(2\frac{\partial u}{\partial x} - \frac{\partial v}{\partial y}\right) \qquad \tau_{yy} = -\frac{2}{3}\mu\left(2\frac{\partial v}{\partial y} - \frac{\partial u}{\partial x}\right) \qquad \tau_{xy} = -\mu\left(\frac{\partial u}{\partial y} + \frac{\partial v}{\partial x}\right) \tag{13}$$

The form of the energy equation in which temperature is the integrated variable [5, Ch XIV] is not appropriate for supercritical fluid analysis since this form assumes a constant specific heat (C_v).

Program Formulation

The above equations are more general than necessary for the present analysis so that a number of non-critical terms were eliminated to improve computational speed.

An advantage in using the internal energy form of the energy equation is that the fluid temperature is almost entirely dependent upon the specific internal energy and only slightly dependent upon density. Therefore, over a relatively wide range of pressures, the relation $T = T(\rho,e)$ was replaced by the computationally simpler function involving only a one-dimensional table interpolation:

$$T = T\ (e) \tag{14}$$

Figure 1 shows this function (obtained from Weber's [8] data) plotted at 55, 60 and 65 atmospheres to indicate the error incurred by neglecting pressure variation in the vicinity of the critical point.

The form of the equation of state shown by eqn. (10) was not available, so that it was necessary to use the equivalent (though for this application computationally less desirable) relation

$$P = P\ (\rho,\ T) \tag{15}$$

which was available in Stewart's equation of state [9]. The relations selected for pressure and temperature are acceptable in that an iterative procedure is not required. However, if pressure is to be computed from temperature, the above approximation to the temperature-energy function may be more critical than if temperature is used only for heat conduction.

The general governing equations assume only that Stokes hypothesis regarding the viscosity coefficients holds, and that thermal radiation/absorbtion effects are insignificant. For the present application, a number of simplifications to these equations are made. First, the velocities developed in the low acceleration environment are so small that the kinetic energy terms in the energy equation may be neglected. Second, the low velocities coupled with the low viscosity of oxygen make the viscous terms in the energy equation negligible. For computational simplicity thermal conductivity and viscosity are assumed constant. The remaining viscous terms are further simplified by assuming that the fluid is incompressible as far as viscous dissipation is concerned.

Incorporating these simplifications in the general equations and rearranging, the governing equations used in this analysis are written.

Continuity

$$\frac{\partial \rho}{\partial t} = - \frac{\partial (\rho u)}{\partial x} - \frac{\partial (\rho v)}{\partial y} \tag{16}$$

X-Component Momentum

$$\frac{\partial (\rho u)}{\partial t} = - \frac{\partial (\rho uu)}{\partial x} - \frac{\partial (\rho uv)}{\partial y} - \frac{\partial P}{\partial x} + \rho g_x + \mu \left(\frac{\partial^2 u}{\partial x^2} + \frac{\partial^2 u}{\partial y^2}\right) \tag{17}$$

Y-Component Momentum

$$\frac{\partial (\rho v)}{\partial t} = - \frac{\partial (\rho vu)}{\partial x} - \frac{\partial (\rho vv)}{\partial y} - \frac{\partial P}{\partial y} + \rho g_y + \mu \left(\frac{\partial^2 v}{\partial x^2} + \frac{\partial^2 v}{\partial y^2}\right) \tag{18}$$

Energy

$$\frac{\partial (\rho e)}{\partial t} = - \frac{\partial (\rho e+P)}{\partial x} - \frac{\partial (\rho e+P)}{\partial y} + k \left(\frac{\partial^2 T}{\partial x^2} + \frac{\partial^2 T}{\partial y^2}\right) + \dot{Q}_v \tag{19}$$

Thermodynamic Relation

$$T = T(e) \tag{20}$$

Equation of State

$$P = P(\rho, T) \tag{21}$$

Typical initial conditions are:

$$\begin{aligned} u(x,y,o) &= 0 \\ v(x,y,o) &= 0 \\ P(x,y,o) &= P_o(x,y) \text{ (specified to balance body forces)} \\ T(x,y,o) &= T_o \\ \rho(x,y,o) &= \rho_o(P,T_o) \\ e(x,y,o) &= e_o(T_o) \end{aligned} \tag{22}$$

Boundary conditions for a closed tank take the form:

$$u(w,y,t) = u(x,w,t) = 0$$
$$v(w,y,t) = v(x,w,t) = 0 \qquad (23)$$
$$\frac{\partial T}{\partial x}(w,y,t) = \frac{\partial T}{\partial y}(x,w,t) = -\frac{q(t)}{k} \text{ (heat leak)}$$

where w indicates a value of x or y at any wall.

The addition of boundary conditions defining a heater and an outlet port is discussed more thoroughly in a following section. Basically, however, the heater is a region of fluid in which internal heat generation is specified, and the outlet port is defined by a normal velocity at a section of the tank wall such that a prescribed mass withdrawal rate occurs. This exit velocity convects mass, momentum, and energy from the system.

FINITE DIFFERENCE FORMULATION

Discussion of Numerical Techniques

A wide variety of finite-difference schemes are available for evaluating the governing equations, and Richtmyer and Morton [4] provides a good source reference. The AIAA reprint series [10] contains an extensive bibliography and a collection of the more interesting recent papers relating primarily to high-speed flow. Numerical methods discussed in Ralston and Wilfe[11], and Cheng[12] summarizes the fundamental principles relating to the numerical solution of the Navier-Stokes equations.

The numerical integration of the governing equations is performed at a finite number of discrete points located throughout the fluid volume. The difference equations are obtained by replacing the partial derivatives with suitable finite-difference approximations typically derived by Taylor-series expansions in space and time. Alternately, the difference equations can be derived directly from fundamental conservation principles applied to a fluid control volume [12]. This method avoids taking the limit as $\Delta V \to 0$ to form the differential equations followed by the reverse process of discretization. The two methods are basically equivalent; however, the latter is quite useful for visualizing and formulating conservative-form difference equations particularly in curvilinear coordinate systems and parameter spaces.

The time variable is discretized and is given by $t^n = n\,\Delta t$. The fluid state is advanced from the (n) time plane to the (n+1) time plane by integration. When the time derivative is approximated by a forward difference, all information used to advance the state to (n+1) Δt is available at the n^{th} time plane. This is the explicit formulation and is equivalent to a step integration procedure. The two-step Lax-Wendroff [4] scheme generates provisional values at $(n + \frac{1}{2})\,\Delta t$ which are used to advance to the (n+1) time plane. This procedure centers the time difference which gives second order accuracy in time.

Various other numerical schemes are available which use weighted averages of data obtained from several time planes (n-1), (n), and (n+1) to obtain the updated value at (n+1). Schemes which require data at the (n+1) time plane to advance the time to (n+1) Δt are implicit and require the simultaneous solution of high-order systems of equations. Efficient relaxation techniques make the implicit formulation quite powerful for certain types of problems.

Most implicit schemes are unconditionally stable for any time step, whereas, explicit schemes are stable only when rather stringent stability conditions are observed. However, explicit schemes are straight forward and require the least computation per time step. The advantage of one scheme over the other depends upon the rate at which the fluid properties are changing. Explicit schemes are preferred for time-dependent problems in high-speed flow and for problems in which wave propagation is important. Implicit schemes are effective for problems in low speed flow and certain steady-state problems. The use of scaling principles to transform the low speed flow problem into one in which the transport mechanisms occur very much faster than in real time appears to be effective in broadening the class of problems which may be solved efficiently using the explicit formulation.

Problems can arise in achieving stability in the explicity-formulated conservation equations. Lax and Wendroff[4] used second-order accurate centered time differences. Rusanov[13] added numerical damping terms to the space differences. Goodrich[14] has shown that the numerical damping terms of Rusanov can be represented by a weighted biasing of the convective difference terms; a method which is similar to the upstream differencing technique used below. Richtmyer[4] has suggested adding pseudo-viscosity terms of the form $a \frac{\partial u}{\partial x} \left| \frac{\partial u}{\partial x} \right|$ to stabilize the momentum equations.

Technique Employed

The technique employed in this analysis is patterned after the method of Courant, Fredricks, and Lewy (1929) for the wave equation[4, p 292]. In this method, the momentum equations are advanced to the (n+1) time plane first, and the updated velocities u^{n+1}, v^{n+1} are then used to advance the continuity and energy equations. By performing the integration in two steps, the continuity and energy equations appear to be semi-implicit, although they are effectively explicit since the necessary information is available from previous calculation. However, when this method is used with centered space differences, physically unrealistic temperature profiles result as fluid convection takes place. Richtmyer[4, p 292] credits the cure for this problem to Lelevier. This solution replaces the centered space differences used for the convective terms by forward or backward space differences as the sign of the convecting velocity is negative or positive. This procedure is quite common and goes by a number of names including upwind or upstream differencing and donor-cell differencing. These differences, however, are only of first order accuracy.

As applied to the grid system used in this analysis, upstream differencing has the effect of defining the values of the convected properties at the control-volume interface as being the values of the upstream cell. Central differencing implies averages of the adjacent cell values at the interface.

Grid System

Grid points are uniformly spaced in the x and y directions at constant intervals $\Delta x = \Delta y = L$. It is convenient to visualize an elemental control volume $\Delta V = \Delta x\, \Delta y\, \Delta z = L^3$, referred to as a cell, surrounding each grid point. According to Cheng [12], "The fluxes must be evaluated on the cell boundary while the conserved quantities are determined only as averages over the cell."

The two- dimensional fluid volume is characterized by several hundred of these cubic cells arranged in a plane. The circular configuration of the oxygen tank crosssection is approximated in a stepwise fashion by removing cells from corners of the rectangular cell grid. For example see Figure 9.

Individual cells are identified by the indicies (i,j) in the x- and y- direction as shown in Figure 2 so that the physical position of the center of cell (i,j) is located at

$$(x_i, y_j) = (i-\tfrac{1}{2})\Delta x,\ (j-\tfrac{1}{2})\Delta y \tag{24}$$

The integrated fluid properties ρ, ρu, ρv, and ρe are identified with each cell center and represent the average properties over the cell volume. The value of a property at the center of cell (i,j) is designated for example as

$$P_{ij} = P(x_i, y_j) \tag{25}$$

For mathematical consistency, the velocities and the thermodynamic properties of the fluid in the cell also are defined at the cell center so that the following relationships can be used:

$$u_{ij} = \rho u_{ij}/\rho_{ij}$$

$$v_{ij} = \rho v_{ij}/\rho_{ij} \tag{26}$$

$$T_{ij} = T\ (\rho e_{ij}/\rho_{ij})$$

$$P_{ij} = P\ (\rho_{ij}, T_{ij})$$

It is convenient to define properties, certain gradients, and convection velocities at the cell walls which lie midway between grid points, and which are indicated by half-subscripts. Convection velocities at these faces are evaluated by linear interpolation:

$$u_{i-\frac{1}{2},j} = \tfrac{1}{2}(u_{i-1,j} + u_{ij}) \tag{27}$$

$$v_{i,j-\frac{1}{2}} = \tfrac{1}{2}(v_{i,j-1} + v_{ij})$$

To achieve upstream differencing for the convection terms, the value of a convected property is defined as the value existing in the upstream cell as determined by the sign of the convecting velocity at the cell interface. Convected properties evaluated in this manner are ρ,ρu,ρv, and $(\rho e + p)$. The result is that the upstream property is convected across the interface at the average velocity. A typical flux at the left face of cell (i,j) is illustrated as

$$\rho_{i-\frac{1}{2},j}\ u_{i-\frac{1}{2},j} \tag{28}$$

The difference in mass flux across cell (i,j) in the x-direction becomes

$$\delta_x(\rho u)_{ij} = \rho_{i+\frac{1}{2},j} u_{i+\frac{1}{2},j} - \rho_{i-\frac{1}{2},j}\ u_{i-\frac{1}{2},j} \tag{29}$$

Since the quantities at cell walls are invarient during calculations at the upstream and downstream cells, local conservation principles are observed identically. Whatever quantity leaves one cell across a cell wall must enter the adjacent cell.

An attempt was made to describe the transition of fluid properties from one cell to the next as a parabola which was biased in the upstream direction.[15] While this scheme was numerically stable, it did not eliminate temperature decreases in cells surrounding the high temperature heater cell.

The pressure gradient across the node is represented by a centered space difference. To accomplish this in the present formulation, the cell wall pressure is defined as an average:

$$P_{i-\frac{1}{2},j} = \tfrac{1}{2}(P_{i-1,j} + P_{i,j}) \tag{30}$$

The resulting pressure difference at cell (i,j),

$$\delta_x P_{ij} = P_{i+\frac{1}{2},\,j} - P_{i-\frac{1}{2},\,j} \tag{31}$$

is identical to the centered pressure difference taken across two cell intervals.

The diffusion terms such as $\frac{\partial^2 T}{\partial x^2}$ and $\frac{\partial^2 u}{\partial x^2}$ are not influenced by fluid convection and usual centered differences are used:

$$\delta_x^2 T_{ij} = T_{i-1,j} - 2T_{ij} + T_{i+1,j} \tag{32}$$

While not employed here due to time limitation, it would be convenient to express the first temperature differences at the cell walls and obtain the second differences as

$$\delta_x^2 T_{ij} = \delta_x T_{i+\frac{1}{2},j} - \delta_x T_{i-\frac{1}{2},j} \tag{33}$$

A temperature-dependent conductivity could be added by a simple extension as:

$$\delta_x(k\,\delta_x T)_{ij} = (k\,\delta_x T)_{i+\frac{1}{2},j} - (k\,\delta_x T)_{i-\frac{1}{2},j} \tag{34}$$

The difference forms of the governing equations employed are shown below along with the necessary supporting equations and definitions. Unless otherwise indicated, data is taken at the n^{th} time plane.

$$\begin{aligned}
\rho u_{ij}^{n+1} &= \rho u_{ij}^{n} + \frac{\Delta t}{\Delta x}\left[-\delta_x \rho uu_{ij} - \delta_y \rho uv_{ij} - \delta_x P_{ij} - \rho_{ij} g_x + \frac{\mu}{\bar{\rho}\Delta x}(\delta_x^2 \rho u_{ij} + \delta_y^2 \rho v_{ij})\right] \\
\rho v_{ij}^{n+1} &= \rho v_{ij}^{n} + \frac{\Delta t}{\Delta x}\left[-\delta_x \rho vu_{ij} - \delta_y \rho vv_{ij} - \delta_x P_{ij} - \rho_{ij} g_x + \frac{\mu}{\bar{\rho}\Delta x}(\delta_x^2 \rho v_{ij} + \delta_y^2 \rho v_{ij})\right] \\
\rho_{ij}^{n+1} &= \rho_{ij}^{n} + \frac{\Delta t}{\Delta x}\left(-\delta_x \rho u_{ij} - \delta_y \rho v_{ij}\right) \\
\rho e_{ij}^{n+1} &= \rho e_{ij}^{n} + \frac{\Delta t}{\Delta x}\left[-\delta_x \rho hu_{ij} - \delta_y \rho hv_{ij} + \frac{k}{\Delta x}(\delta_x^2 T + \delta_y^2 T)\right]
\end{aligned} \tag{35}$$

Typical quantities used in the above equations are illustrated below in the x-direction. Quantities relating to the y-direction are analogous.

$$\rho h_{ij} = \rho e_{ij} + P_{ij} \tag{36}$$

$$\delta_x \rho u_{ij} = \rho_{i+\frac{1}{2},j} u^{n+1}_{i+\frac{1}{2},j} - \rho_{i-\frac{1}{2},j} u^{n+1}_{i-\frac{1}{2},j}$$

$$\delta_x \rho uu_{ij} = \rho u_{i+\frac{1}{2},j} u_{i+\frac{1}{2},j} - \rho u_{i-\frac{1}{2},j} u_{i-\frac{1}{2},j} \tag{37}$$

$$\delta_x \rho vu_{ij} = \rho v_{i+\frac{1}{2},j} u_{i+\frac{1}{2},j} - \rho v_{i-\frac{1}{2},j} u_{i-\frac{1}{2},j}$$

$$\delta_x \rho hu_{ij} = (\rho e_{i+\frac{1}{2},j} + P_{i+\frac{1}{2},j})\, u^{n+1}_{i+\frac{1}{2},j} - (\rho e_{i-\frac{1}{2},j} + P_{i-\frac{1}{2},j})\, u^{n+1}_{i-\frac{1}{2},j}$$

$$\delta_x^2 \rho u_{ij} = \rho u_{i-1,j} - 2\rho u_{ij} + \rho u_{i+1,j} \tag{38}$$

$$\delta_x^2 \rho v_{ij} = \rho v_{i-1,j} - 2\rho v_{ij} + \rho v_{i+1,j}$$

$$u^{n+1}_{i+\frac{1}{2},j} = \tfrac{1}{2}\left(\frac{\rho u^{n+1}_{i+1,j}}{\rho^{n}_{i+1,j}} + \frac{\rho u^{n+1}_{ij}}{\rho^{n}_{ij}}\right) \tag{39}$$

$$P_{i+\frac{1}{2},j} = \tfrac{1}{2}(P_{ij} + P_{i+1,j}) \tag{40}$$

If $u_{i+\frac{1}{2},j} > 0$	If $u_{i+\frac{1}{2}} < 0$ (41)
$\rho_{i+\frac{1}{2},j} = \rho_{ij}$	$\rho_{i+\frac{1}{2},j} = \rho_{i+1,j}$
$\rho u_{i+\frac{1}{2},j} = \rho u_{ij}$	$\rho u_{i+\frac{1}{2},j} = \rho u_{i+1,j}$
$\rho v_{i+\frac{1}{2},j} = \rho v_{ij}$	$\rho v_{i+\frac{1}{2},j} = \rho v_{i+1,j}$
$\rho e_{i+\frac{1}{2},j} = \rho e_{ij}$	$\rho e_{i+\frac{1}{2},j} = \rho e_{i+1,j}$
$P_{i+\frac{1}{2},j} = P_{ij}$ (work terms)	$P_{i+\frac{1}{2},j} = P_{i+1,j}$

Stability Conditions

Stability of finite-difference equations is discussed in detail in Richtmyer and Morton.[4] The basic requirements for a stable differencing scheme is that the difference equations converge to the differential equations in the limit as $\Delta x \to 0$, $\Delta t \to 0$ which implies that disturbances in the solution decay with time. Stability constraints limit the maximum time increment (Δt) permissible.

The difference analogs of the Navier-Stokes equations are too complex to be fully analyzed with current stability analysis methods. The standard procedure is to evaluate the stability of the hyperbolic and the parabolic terms separately and to use the more restrictive of the two stability constraints.

In the explicit formulation of the Navier-Stokes equations, the hyperbolic limit is usually the most restrictive and results in the stability condition

$$(|u| + c)\,\frac{\Delta t}{\Delta x} \leq 1 \tag{42}$$

where u is the fluid velocity and c is the local adiabatic speed of sound. If $u << c$, the condition may be interpreted as limiting the propagation of a pressure wave to the distance of one space increment during a time step Δt.

For a two-dimensional problem, the stability condition becomes

$$(|\vec{u}| + c)\,\frac{\Delta t}{\Delta x} \leq \frac{1}{\sqrt{2}} \tag{43}$$

In the present problem, under the conditions being considered, the speed of sound is about 2500 ft/sec. With a grid spacing of $\Delta x = .1$ ft. the theoretical stability limit gives $\Delta t = .283 \times 10^{-4}$ sec.

Modification For Tank Stretch

Tank stretch affects the fluid state primarily by changing the density of the fluid properties. The work done on the boundaries changes the internal energy and also must be included.

During a tank expansion, the mass residing in an arbitrary volume becomes distributed throughout a larger volume. In the present Eulerian formulation, it is very difficult to adjust the x-y fluid boundaries to achieve this volume increase. The change was taken up in the z direction

by permitting the unit depth to increase. Since no fluid crosses a node boundary during such an expansion, the mass (m) in the volume is unchanged.

Multiplying through by the node volume, $V=L^2L_z$, the continuity equation on a mass basis becomes:

$$\frac{\partial m}{\partial t} = \frac{\partial \rho V}{\partial t} = -V\left(\frac{\partial \rho u}{\partial x} + \frac{\partial \rho v}{\partial y}\right) \tag{44}$$

Upon discretizing the time variable and introducing the forward time difference, the equation becomes:

$$\frac{m^{n+1}-m^n}{\Delta t} = \frac{\rho^{n+1}V^{n+1}-\rho^n V^n}{\Delta t} = -V^n\left(\frac{\partial \rho u}{\partial x} + \frac{\partial \rho v}{\partial y}\right) \tag{45}$$

Finally, dividing by $\frac{V^{n+1}}{\Delta t}$ and rearranging,

$$\rho^{n+1} = \frac{V^n}{V^{n+1}}\left[\rho^n + \Delta t \left(\frac{\partial \rho u}{\partial x} + \frac{\partial \rho v}{\partial y}\right)\right] \tag{46}$$

The above volume ratio is represented as

$$C_{str} = \frac{V^n}{V^{n+1}} = \frac{V^n}{V^n + \Delta V} \tag{47}$$

where

$$\Delta V = \frac{dV}{dP}\,\bar{\Delta P} \tag{48}$$

$\bar{\Delta P}$ = change in average tank pressure during Δt.

The same argument can be used to develop the expressions for the momentum and energy equations. However, the rate of work done on the boundary during an expansion must be included in the energy equation.

$$\frac{dW}{dt} = PL^2\frac{dL_z}{dt} = P\frac{dV}{dt} \tag{49}$$

Upon discretization

$$\frac{\Delta W}{\Delta t} = P \frac{\Delta V}{\Delta t} \tag{50}$$

Next, dividing by $\frac{V^{n+1}}{\Delta t}$ as before, the work done per unit volume during Δt becomes:

$$\frac{\Delta W}{V^{n+1}} = \frac{P\Delta V}{V^{n+1}} = P \frac{V^{n+1}-V^n}{V^{n+1}} \tag{51}$$

or

$$\frac{\Delta W}{V^{n+1}} = P \left(1- \frac{V^n}{V^{n+1}}\right) \tag{52}$$

and finally,

$$\frac{\Delta W}{V^{n+1}} = P \left(1-C_{str}\right) \tag{53}$$

Since this is the work done on the boundary by the fluid, it must be subtracted from the available internal energy in the cell.

The conservation equations modified for tank stretch are collected together below in a form showing just the time differences:

$$\begin{aligned}
\rho^{n+1} &= C_{str} \left[\rho^n + \Delta t \left(\frac{\partial \rho u}{\partial x} + \frac{\partial \rho v}{\partial y}\right)\right] \\
\rho u^{n+1} &= C_{str} \left[\rho u^n + \Delta t \left(\ldots \quad\right)\right] \\
\rho v^{n+1} &= C_{str} \left[\rho v^n + \Delta t \left(\ldots \quad\right)\right] \\
\rho e^{n+1} &= C_{str} \left[\rho e^n + \Delta t \left(\ldots\right)\right] - \bar{P} \left(1-C_{str}\right)
\end{aligned} \tag{54}$$

where the average tank pressure $\bar{P}$ is used for the work term.

For computational reasons, C_{str} lags by one time step the above calculations so that in reality it is defined as:

$$C_{str} = \frac{V^{n-1}}{V^n} \tag{55}$$

NUMERICAL BOUNDARY CONDITIONS

Boundary Location

Consistent with the control-volume concept, solid boundaries were located at the outward-looking faces of the boundary cells. This location has distinct advantages in simplifying the definition and imposition of boundary conditions.

The alternative to this formulation (i.e. placing boundary mesh points at the wall surface) creates problems in evaluating the fluid properties at the wall, and global conservation may not be observed computationally. In this context, Roache and Mueller[16] cited the difficulty of imposing adiabatic (and therefore any chosen heat flux) conditions at the wall. They also observed that non-conservative methods used to define the wall density led to slow but continuous mass loss in a flow problem over a backstep.

The procedure of defining flux quantities and convection velocities at cell faces further simplifies the imposition of boundary conditions, and permits a unified application of the conservation equations to both interior and boundary cells. This procedure also avoids the use of imaginary grid points located outside the fluid boundary defined by reflection principles. The present method is considerably simpler to apply when flow obstructions or wall irregularities are considered.

Boundary Values

Convection velocities are set to zero at boundary surfaces thus assuring strict global conservation for convective terms. Pressure at the wall, which is necessary only for the momentum equations, is obtained by linear extrapolation from the first two normal interior grid points. Thermal boundary conditions take advantage of the fact that the heat leak is more accurately known than the temperature of the inner tank wall. When calculated at a boundary cell, temperature difference equations are employed which make use of the relations

$$\left.\frac{\partial T}{\partial x}\right|_{wall} = -\frac{q_{x\ leak}}{k} \qquad \left.\frac{\partial T}{\partial y}\right|_{wall} = -\frac{q_{y\ leak}}{k} \tag{56}$$

where $q_{x\ leak}$ and $q_{y\ leak}$ are the boundary heat fluxes obtained by distributing the known heat leak rate $\dot{Q}_{leak}$ uniformly over the exposed surface area. This formulation identically satisfied the global energy

balance and avoids the difficulty in defining the thermal boundary condition discussed by Roach and Mueller.[16]

Separate equations are used at boundary cells to evaluate the viscous dissipation terms in the momentum equations. For example, instead of the centered second difference terms used at interior cells which have the form:

$$(\delta_x^2 \rho u)_{ij} = (\rho u_{i-1,j} - 2\rho u_{ij} + \rho u_{i+1,j}) \tag{57}$$

forward and backward second differences are employed which make use of the zero velocity conditions at the wall:

$$\begin{aligned} (\delta_x^2 \rho u)_{ij} &= (-3\,\rho u_{ij} + \rho u_{i+1,j}) \text{ at left wall} \\ (\delta_x^2 \rho u)_{ij} &= (\rho u_{i-1,j} - 3\rho u_{ij}) \text{ at right wall} \end{aligned} \tag{58}$$

Boundary conditions are imposed at the exterior face of cell (20, 10) such that the prescribed mass withdrawal rate occurs. Since the sign of the convection velocity $u_{20\frac{1}{2},10}$ must be positive, the necessary quantities at the cell wall (P, ρ, ρu, ρv, and ρe) are obtained by linear extrapolation of the form

$$\rho_{i+\frac{1}{2},j} = \tfrac{1}{2}(-\rho_{i-1,j} + 3\rho_{ij}) \tag{59}$$

The necessary convection velocity is obtained from the mass flow relation $\dot{m}=\rho A u$ as

$$u_{20\frac{1}{2},10} = \frac{\dot{m}}{\rho_{20\frac{1}{2},10} L^2} \tag{60}$$

With the cell wall quantities thus defined, the difference equations are applied at the outlet port cell as at any other cell. The convection of mass, x- and y- momentum, and enthalpy from the system takes place automatically.

SCALING PRINCIPLES

Computational stability considerations place stringent requirements on the permissible size of the time step (Δt) required to integrate the governing equations in the explicit formulation. The time step is determined by the time interval required for a pressure wave to propagate the distance of one cell. Time steps of this order are required for problems in high-speed flow or for problems in which pressure wave propagation contributes significantly to the solution. In the present problem, wave propagation may be of importance if fluid oscillations following a G-spike are of sufficient magnitude to destroy thermal gradients generated by heater operation under a low-g environment.

However, fluid heating and stratification occur on a time scale very much larger than that of wave motion, and the resulting computer time required to simulate an appropriate duration of flight is excessive. For this reason it was necessary to introduce scaling principles to transform the original problem into an equivalent scaled problem in which certain mechanisms of importance occur in the scaled time very much faster than in real time. Since non-linear real gas properties are used to describe the fluid temperature and pressure, the thermodynamic state cannot be scaled easily. Therefore, the conditions governing thermal stratification and fluid mixing are adjusted so that these mechanisms operate in scaled time. The desired rates of heating, fluid withdrawal, and fluid motion are increased such that the resulting pressures and temperatures remain unaltered at corresponding times in the scaled and unscaled systems.

The specific heat (C_v), pressure (P), temperature (T), and density (ρ) are not altered. However, the transport constants, thermal conductivity (k) and absolute viscosity (μ), are adjusted as required. Since the values of μ and k for supercritical oxygen are small and do not dominate the stratification and mixing mechanisms, these parameters are considered constant. Therefore, the following principles have been applied. The scale factor is designated by s, and the subscript s represents a value appearing in the scaled system such that the real time t is given by

$$t = st_s \tag{61}$$

The following constraints have been placed upon the scaled system:

$$\begin{aligned} \rho_s &= \rho \qquad \text{(density)} \\ T_s &= T \qquad \text{(temperature)} \end{aligned} \tag{62}$$

$$(C_p)_s = C_p \qquad \text{(specific heat)}$$

$$L_s = L \qquad \text{(characteristic length)}$$

Since it is desired that the flow processes occur more rapidly,

$$\begin{aligned} u_s &= su && \text{(x velocity)} \\ v_s &= sv && \text{(y velocity)} \\ q_s &= sq && \text{(heat flux)} \\ \dot{m}_s &= s\dot{m} \text{ mass flow rate} && \text{(mass flow rate)} \end{aligned} \tag{63}$$

The similarity parameters which apply are:

$$\text{Reynolds Number} \qquad R_e = \frac{\rho VL}{\mu} = \frac{\text{inertial forces}}{\text{viscous forces}}$$

$$\text{Prandtl Number} \qquad P_r = \frac{C_p \mu}{k} = \frac{\text{heat generation}}{\text{heat conduction}}$$

$$\text{Nusselt Number} \qquad N_u = \frac{qL}{k\Delta T} = \frac{\text{total heat transfer}}{\text{conductive heat transfer}}$$

$$\text{Grashof Number} \qquad G_r = \frac{\rho^2 g \beta \Delta T\, L^3}{\mu^2} = \frac{\text{bouyant forces}}{\text{viscous forces}}$$

To maintain similarity of R_e, μ is scaled as:

$$\mu_s = s\mu. \tag{64}$$

Similarity of both P_r and N_u require that:

$$k_s = sk. \tag{65}$$

Recognizing that the heat diffusion rate must be scaled, the requirement placed upon k can be obtained directly from the definition of the thermal diffusivity.

$$\alpha_s = s\alpha = s\left(\frac{k}{\rho C_p}\right). \tag{66}$$

Since the compressibility (β) remains unchanged by the initial constraints, to maintain Grashof number similarity, the acceleration must be scaled as:

$$g_s = s^2 g. \tag{67}$$

It should be emphasized that this scaling procedure speeds up the physical processes occurring in the fluid without disturbing the thermodynamic properties of the fluid itself. To accomplish this, it is necessary to adjust only the transport properties μ and k. In particular, the properties which determine the sonic velocity in the fluid have been preserved. The basic purpose for scaling is to increase the ratio of the fluid velocity to the sonic velocity (Mach number) because the sonic velocity of the explicit numerical solution limits the size of the permissible computation time steps.

Verification of this scaling procedure was performed by comparing temperature and velocity profiles taken at corresponding times from computer runs in which differing scale factors are used. In addition, good results were obtained for the Apollo 12 pressure collapse and heater cycle simulations in which scale factors of 2400 and 6000 were employed.

The increase in acceleration required to maintain the Grashof number in the scaled solution affects the required hydrostatic pressure distribution and, therefore, the distribution of the fluid mass. However, for problems involving a low-G environment, a scale factor which permits a reasonable simulation time gives rise to a negligibly small fictitious pressure gradient.

It appears that the maximum valid scale factor is restricted by the magnitude of the acceleration. Figure 3 shows the relative increase in hydrostatic pressure from the center of the tank to the tank wall necessary to counteract the scaled gravitational body forces. At a given G-level, experimentation indicates that a scale factor that produces a 1% pressure increase does not alter the convection or thermodynamic behavior observed in the Apollo 12 simulation. It should be cautioned that scaling amplifies fluid-dynamic start-up transients resulting from imprecisely known initial conditions (eg. the velocity profile around the outlet port), so that additional scaling restrictions must be considered.

In addition, it should be noted that stability conditions relate permissible time steps to thermal conductivity and to fluid viscosity. However, these constraints are less restrictive of the scale factor than the G-constraint for the present problem.

NUMERICAL RESULTS

Natural Convection in a Rectangular Enclosure

A test case in natural convection was run and the results are compared with an incompressible solution of a similar problem obtained by Wilkes and Churchill.[17]

A two-dimensional rectangular enclosure containing an incompressible fluid is oriented in a vertical plane with respect to the gravity vector. The left wall is held at a constant temperature T_1, and the right wall is held at a higher temperature T_2 also assumed constant. The other two walls are insulated. Initially, the fluid is at rest and at a temperature equal to the average of the boundary wall temperatures. The problem is to find the fluid velocity components and temperature at points throughout the fluid as steady-state conditions are approached.

As heat conduction takes place, a negative horizontal density gradient develops. The resulting unbalanced vertical buoyant forces cause two vortices to form with a net counter-clockwise rotation of the fluid. As the flow continues, the density gradient deforms and the two vortices eventually merge into one due to the viscous dissipation of momentum. As steady-state conditions are approached, the moment produced by the viscous forces acting at the walls balances the net buoyant moment.

Wilkes and Churchill introduced the vorticity and stream functions into the non-dimensionalized equations of motion. A linear density dependence upon temperature was used to produce the essential density gradients for natural convection. An implicit alternating direction technique was used to advance the time-dependent solution toward steady state. Figures presented[17] show the stream function and isotherms at several times including steady state. The dimensionless conditions associated with these figures are: $P_r = .733$, $G_r = 20{,}000$, $N_n = 2.874$.

The formulation used in the present solution necessitated two modifications to the problem. First, fluid compressibility was introduced in order to compute pressure explicity in terms of temperature and density. The ideal gas relation was assumed for this purpose. Second, the constant-temperature boundary conditions were changed to constant-heat-flux boundary conditions to be compatible with the model capability developed for simulation of heat leak into the Apollo oxygen tank.

The compressibility modification had a negligible effect on the solution since the vertical pressure differential was kept small with respect to the bulk fluid pressure. The second modification resulted in observable differences in the temperature profiles near the vertical walls. However, the basic character of the temperature profile away from these walls is preserved, and the resulting velocity profiles are similar to those obtained by Wilkes and Churchill.

The fluid properties, heating rate, and acceleration were adjusted so that the proper boundary temperatures were approached at steady-state. The final dimensionless quantities achieved were: Pr = .611, Gr = 21,000, and Nu = 3.88 which are in reasonable agreement with the Wilkes and Churchill values and yielded similar results. These values were computed using the average extrapolated wall temperatures.

A 10 x 10 cell grid was used to describe the fluid volume. Dimensions of the square enclosure, the bulk density, and the compressibility of the fluid were selected to yield a problem in which heating and fluid motion took place rapidly in real time in order to minimize computer time. Problem conditions are shown in Figure 4.

Figure 5a is a computer-generated velocity vector plot which shows the two initial counter-clockwise rotating vortices after 1/2 second of flow development. Figures 5b and 5c show the two vortices merging into one and the development of circularized flow. Figure 5d shows the essentially steady velocities at 4.95 seconds. Figure 6 shows the same vector plot at 4.95 seconds on which the dimensionless stream function obtained from the Wilkes and Churchill solution has been superimposed. Steady-state temperature profiles at ten horizontal cross-sections and fluid isotherms are shown in Figures 7 and 8. The general shape of the isotherms is in good agreement with the dimensionless isotherms of Wilkes and Churchill.

It is important to note the difference in the thermal boundary conditions. Isotherms cannot intersect the constant temperature walls used by Wilkes and Churchill. However, to maintain a uniform heat flux at the wall as assumed in the present solution, the wall temperature must vary in the vertical direction and isotherms intersect these walls as shown. Although the present results cannot be compared directly with those of Wilkes and Churchill, the general character of the solutions appears to be in reasonable agreement.

It is interesting to note that starting from zero, the fluid rotation rate passes through a maximum before approaching the steady-state rate. This phenomenon is the result of the inertial lag in responding to a change in heat flux at the walls (as occurs at t = 0). During this lag, high temperature and low temperature fluid masses accumulate near the respective walls, resulting in an over-acceleration of the fluid. The bulk rotation rate then builds up to a maximum and carries the heated and cooled fluid elements across the vertical centerline. At this point, a net counter-acting moment develops which retards the bulk rotation, and the steady-state rate is approached asymptotically.

Apollo 12 Pressure Collapse Simulation

The program was operated for flight conditions to demonstrate capability to simulate the stratification and mixing of supercritical oxygen which takes place under a flight-type acceleration environment. These conditions are shown in Figure 9 and are approximately those of the Apollo 12 mission at 7:30 GET. The density corresponds to the 95% tank quantity.

The heat added to the fluid cross section was input at cell (12,10) as shown in Figure 9. This single heater cell represents a heater boundary layer volume of 1.73 cubic inches. The rate of oxygen withdrawal was 1.4 lbm/hr. The outlet port was the exterior face of cell (20,10). The pressure limits for the heater switch were set at 860 and 900 psi so that the heater cycled automatically keeping the bulk pressure within a 40 psi dead band. A constant acceleration of 2×10^{-8} G's was applied in the -Y direction. At a simulation time of 70.5 minutes, an acceleration step to 10^{-4} G's was applied in the -X direction and the heater was turned off. The scale factor of 2400 was used in this simulation to achieve a computer time to simulation time ratio of 5/1 using a program time step of $.5 \times 10^{-4}$ seconds.

Figure 10 shows the stratified tank pressure (upper curve) and the equilibrium pressure (lower curve) as functions of time. The simulation started from equilibrium conditions. The equilibrium pressure rise rate was 3.7 psi/minute and the decay rate was -3.8 psi/minute. After 70 minutes of stratification, the minimum potential pressure collapse developed was 80 psi. The general divergence of the two curves shows that a quasi-steady state pressure collapse potential had not been reached after 70 minutes of stratification. The time required for the first complete heater cycle is about 12 minutes. The cycle time for

succeeding cycles decreased to about 3 minutes per cycle which is about one-third the time required for a flight heater cycle under similar conditions. The inclusion of tank stretch would about double this cycle time. The maximum temperature reached in this simulation was 287°R at the heater node. Negligible fluid convection occurred in the vertical direction.

Figure 11 shows the tank pressure decaying toward the equilibrium pressure in response to the G-step to 10^{-4} G's at 70.5 minutes simulation time. Fluid oscillations in the tank caused by the G-step and accentuated by scaling have been smoothed. The pressure decay observed in the Apollo 12 data at 8:36 GET also is shown for comparison.

Apollo 12 Heater Cycle Simulation

Following the relatively successful initial simulation which demonstrated thermal stratification with ensuing pressure collapse, it was decided to incorporate refinements to the idealized model in an effort to more accurately predict the heater cycle times. These refinements included the effects of tank stretch, line compression, heater thermal mass, and heater radiation to the tank wall.

Under similar environment and initial conditions but with somewhat more rigorously defined heating and mass flowrates, a second Apollo 12 simulation was undertaken which incorporated the above refinements. The time step of $.25 \times 10^{-4}$ seconds as indicated by stability conditions was observed even though a time step twice as large did not appear to alter the numerical stability. The problem was scaled by a factor of 6000 so that 60 minutes of simulation time was covered by 0.6 seconds of solution time. The associated computer time was three hours resulting a computer time/real time ratio of 3/1 on the 1108 system at the NASA-MSC computing center. Considering the change in scale factor and the smaller time steps taken, revisions made to the program allow it to run two times faster than it did for the first Apollo 12 simulation.

Figure 12 shows the resulting computed tank pressure history. Pressure switch limits were set at 860 and 900 psi. The run was performed in a number of segments using the program re-start capability. At the beginning of the second and third segments at 13.5 and 23 minutes the heater switch was inadvertently reset to the "on" position which accounts for the fact that the pressure does not decay to the lower pressure limit at the end of the first two cycles.

The fact that the tank stretch and other refinements do indeed lengthen the heater cycle times may be seen by comparing Figures 10 and 12. The heater cycle time appears to be around 12 minutes which agrees well with the 13 minute cycle time predicted from Figure 3.4.10 of the Apollo Handbook.[1]

The effect of heater thermal mass is observed to cause pressure excusions beyond the pressure limits and a rounding of the pressure peaks. The developed shape of the pressure decay from the peak is due to the decay of the local high temperature at the heater node followed by the more gradual decay resulting from the general fluid expansion caused by mass withdrawal. The highest temperature reached by the fluid in the heater node was 293°R.

In this problem, fluid convection was virtually non-existent. After one hour of simulation, the only apparent migration of the fluid was toward the outlet port which is located perpendicular to the acceleration vector. Therefore, under $2x10^{-8}$ G's these results indicate that conduction is the primary heat transfer mechanism.

Acceleration Effects

The above Apollo 12 simulation was repeated but under an acceleration of $-2x10^{-5}$ G's - two orders of magnitude higher - to illustrate the effects of acceleration on convection velocities. Employing a scale factor of 2400, the simulation was run to 11.5 minutes by which time a maximum convection velocity of $.35x10^{-3}$ ft/sec had developed at the heater node. Figure 13 shows a velocity vector plot of the convection pattern developed by time. Density and temperature data indicate that the heated fluid migrated a distance of about 1-1/2 cells or 1.8 inches which corresponds to an average velocity of about $.2x10^{-3}$ ft/sec.

Scaling Verification

It was tacitly assumed in the discussion of scaling procedures that all the transport process would in fact take place in scaled time. Also assumed was that the pressure and temperature distributions would not be altered by the scaling procedure.

The Apollo 12 convection problem just described was repeated using a scale factor of 4800 instead of 2400. Comparisons of the data from the two cases indicate that the temperature profiles and pressure rise rates are preserved. At a scaled time of 5 minutes for both cases the tank pressures agreed within 1 psi and the heater cell temperatures agree within 1°R after rising 53°R during heater operation. Scaled fluid

velocities in the second case (scale factor = 4800) are just double the scale velocities of the first case (scale factor = 2400) as required. Upon descaling, the actual fluid velocities obtained from the two scaled systems are the same, and the scaling procedure is verified.

Evidence supporting the scaling procedure also can be inferred from the quality of the Apollo 12 simulations which were scaled between 3 and 4 orders of magnitude.

High Heat Leak and Boundary Roughness

The circular cross sectional geometry of the Apollo oxygen tank was approximated in a step-wise fashion. A test case was performed to investigate the affect of such a boundary on the flow pattern. In this case, high heat leak of 2000 BTU/hr was imposed at the fluid boundary. This rate corresponds to the limiting heat leak that would occur if the annulus vacuum were lost.[3] An acceleration level of 10^{-5} G's was imposed in the -y direction, and the scale factor of 4800 was used.

The velocity vector plots in Figure 14 show the natural convection after 10, 20, and 32.5 minutes of simulation. The maximum velocity indicated is 10^{-5} ft/sec. Figure 14c shows that local flow distortions are introduced at the protruding corners. This surface roughness probably makes this approach unsuitable for investigations involving tank rotation.

SUMMARY

The conservation equations governing the motion of a compressible viscous fluid were solved in two dimensions using an explicit finite-difference technique. The difference equations were formulated in terms of control-volume grid cells which simplified the imposition of heat flux boundary conditions and assured computational observance of local and global conservation principles. This system also permitted the unified application of the difference equations to both interior and boundary cells without resorting to exterior cells and reflection principles. Real-fluid properties describing the thermodynamic behavior of supercritical oxygen were used so that the pressure collapse phenomenon could be observed in the Apollo oxygen Cryogenic Storage System operating under low - G conditions.

The numerical procedure was applied to the simulation of thermal stratification and fluid mixing in the Apollo oxygen storage tank.

The convex tank geometry was approximated by removing the corner cells of a rectangular cell grid. Wall boundary conditions were adjusted at one cell face to emit a prescribed mass flowrate. Electrical heater input was treated as local internal heat generation. The effects of heater thermal mass and radiation to the tank were included. The effect of tank stretch and line compression on dP/dt was modeled as an out-of-plane fluid expansion. Scaling principles were invoked to achieve acceptable computer execution times for reasonable flight durations.

A verification test case was performed involving heat transfer and natural convection in a vertically-oriented rectangular volume. The convection pattern and isotherms are in good agreement with another numerical solution.

A simulation of stratification and mixing occurring around 7:30 GET in the Apollo 12 mission was presented. Natural convection under 2×10^{-8} G's acceleration was shown to be negligible. The pressure collapse of about 75 psi following a simulated vehicle maneuver is compared with flight data with good results.

Modifications in the heater characterization along with tank stretch effects were shown to significantly improve the simulation of heater cycle operation. A number of additional cases were presented to show the effects of higher acceleration on convection velocities to verify the scaling techniques employed and to evaluate the effects of boundary roughness on convection patterns.

The results obtained for these initial test cases indicate the general capability of this analysis. Unfortunately, time limitations prevented the refinement of certain empirical considerations which would further improve the accuracy of the Apollo simulations.

Future Developments

It has been observed that the finite-difference solution of partial differential equations is limited more by currently available theoretical understanding than by computer capability.[4] However present computers, which perform all operations serially, are not particularly well adapted to computing finite-difference solutions which proceed in a series-parallel fashion. It seems reasonable that the multi-processing capability of present machines will be extended to parallel processing within the same computer program. Such is the thrust of the new multi-computing system at the University of Illinois.[18] This system, called ILLIAC IV, consists of 64 independent processors which operate in unison. By using parallel processing, computer run time can be reduced by a factor of 64. Thus it appears certain that next generation computers of this type will significantly increase the capability of finite difference solutions in multiple space dimensions.

NOMENCLATURE

Symbol	Description
C_{lag}	heater on/off ramps ($0 \leq C_{lag} \leq 1$)
C_{rad}	heater radiation factor ($0 \leq C_{rad} \leq 1$)
C_{str}	tank stretch factor ($= V^{n-1}/V^{n}$)
C_{vol}	model/actual volume ratio (Apollo 12 = .075)
e	internal energy per unit mass
E	total energy per unit mass ($= e + \frac{1}{2}(u^2 + v^2)$)
g	gravitational acceleration
k	thermal conductivity
P	pressure
q	heat flux
$\dot{Q}$	internal heat generation rate
$\dot{Q}_{leak}$	boundary heat leak rate
$\dot{Q}_{v}$	internal heat generation rate per unit volume
t, Δt	time, time increment
T	temperature
u	velocity, x-component
v	velocity, y-component
V	tank volume
μ	absolute viscosity
ρ	density
ρe	internal energy per unit volume
ρu	momentum, x-component
ρv	momentum, y-component
Δx, Δy, L	node dimensions
τ	shear stress
Subscript	
i	x-direction index
j	y-direction index
x	x-component
y	y-component
Superscript	
n	time step index

Figure 1 Oxygen Temperature - Energy Relation

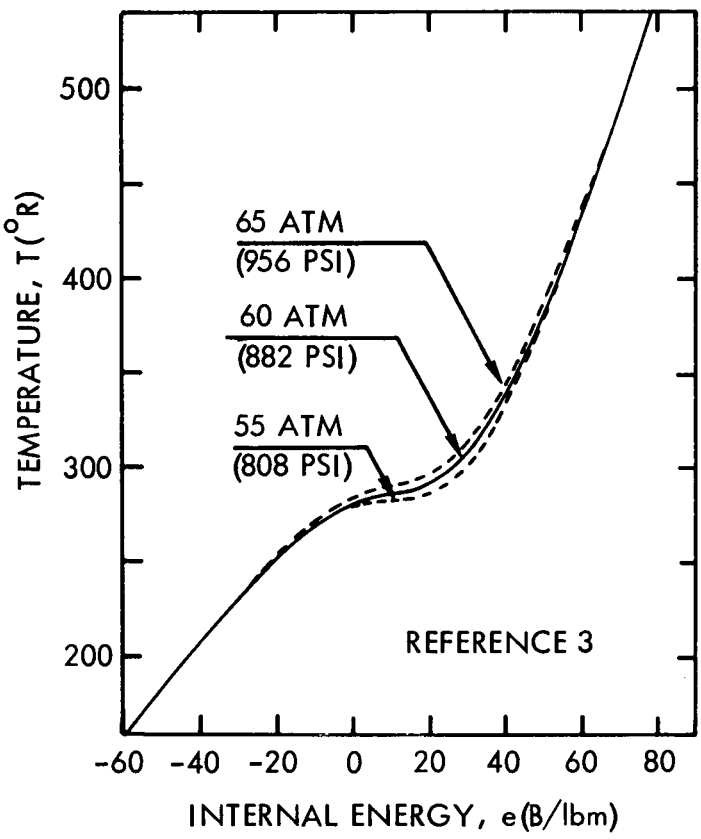

Figure 2 Grid System and Indexing Procedure

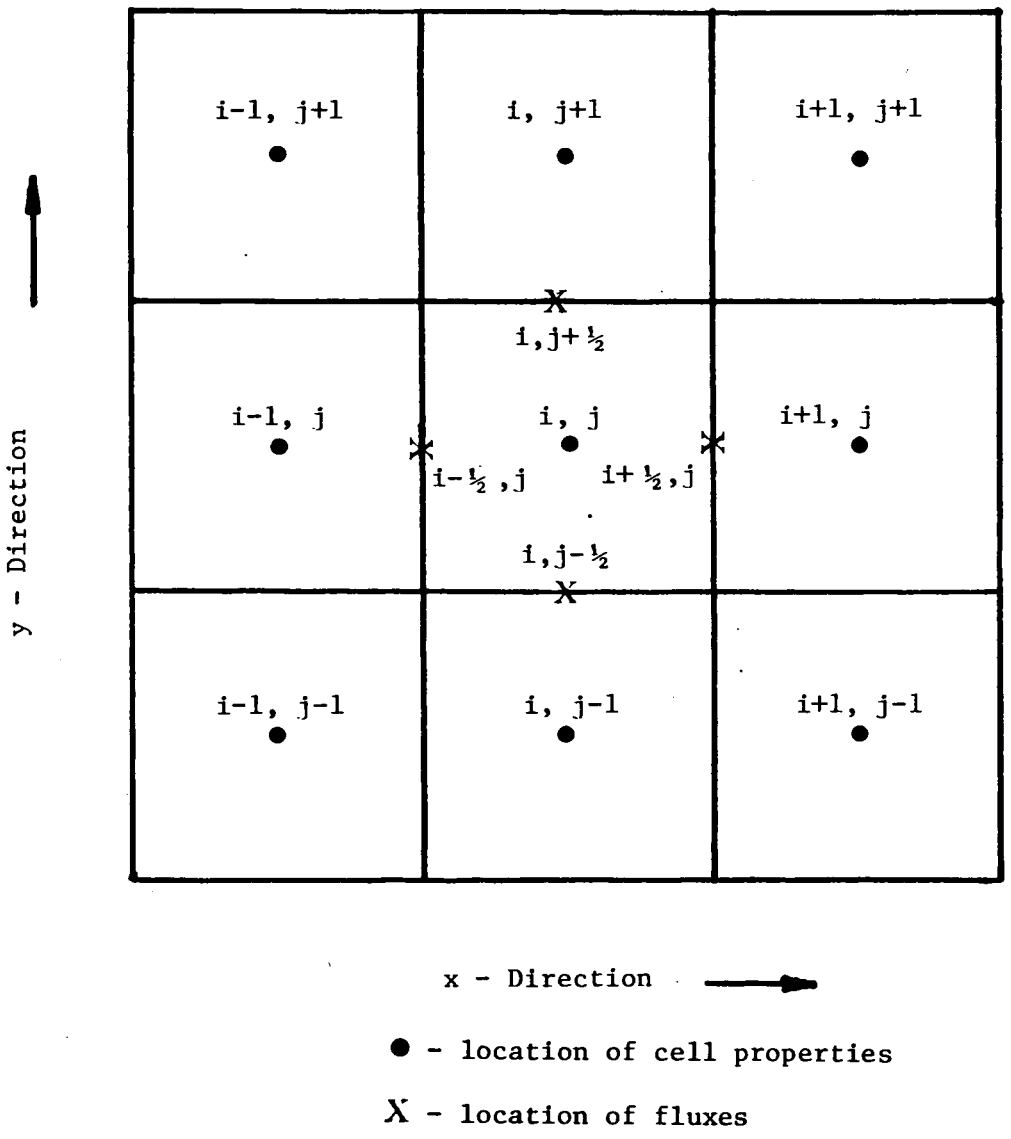

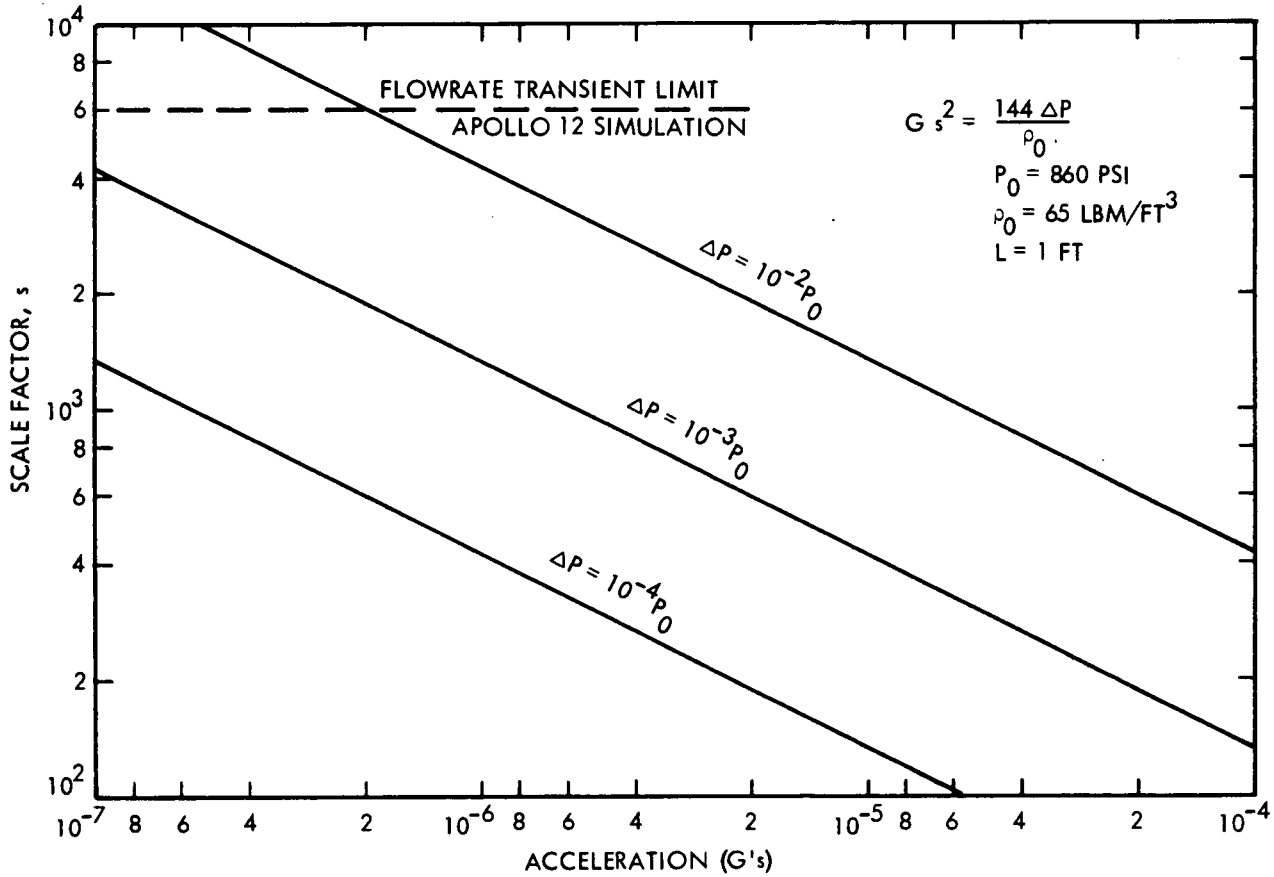

Figure 3 Scale Factor vs Acceleration

Figure 4 . Natural Convection Conditions

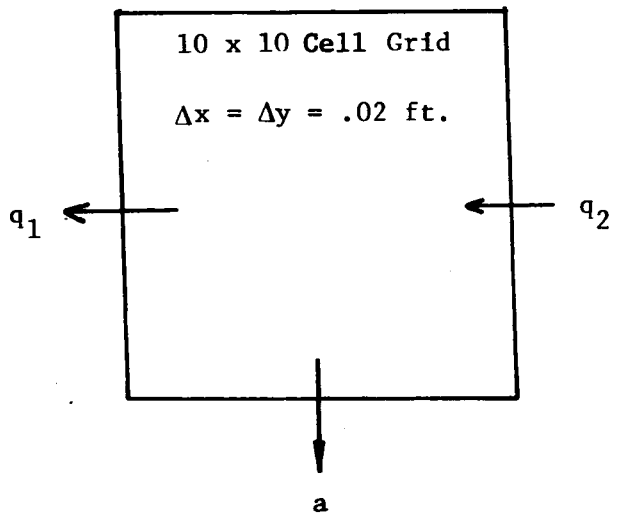

Initial Conditions

$u = v = 0$

$T_o = 100\ ^oR$

$P_o = 500$ psi

$\rho_o = 49.71$ lbm/ft^3

$z = .3$

MW = 32. lbm/lbm-mole

$C_v = .2$ B/lbm-^oR

$\mu = .45$ Poise

$k = 39$ B/ft-hr-^oR

Boundary Conditions

$q_1 = q_2 = .3$ B/ft^2-sec

$u_{wall} = v_{wall} = 0$

a = 8 G's

Figure 5 Natural Convection

a. Initial Vorticies

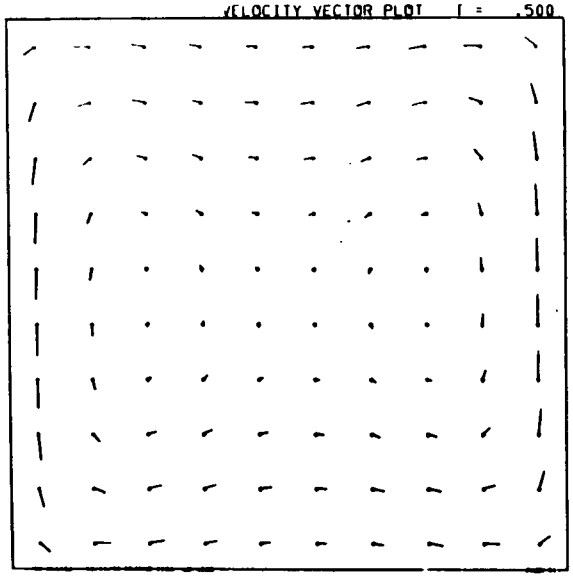

b. Vorticies Merging

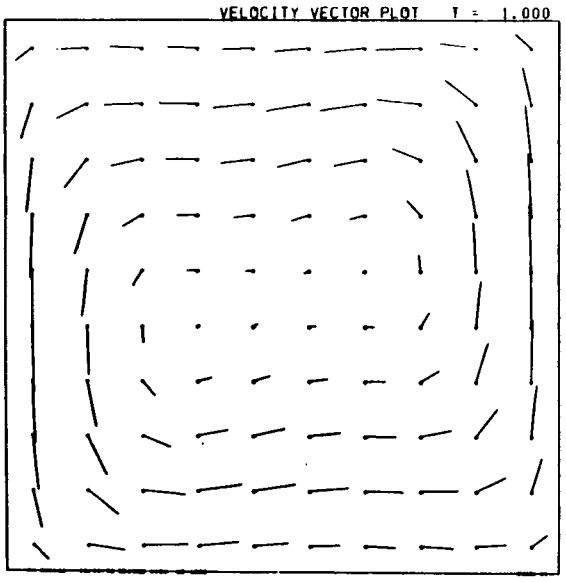

c. Circularized Flow

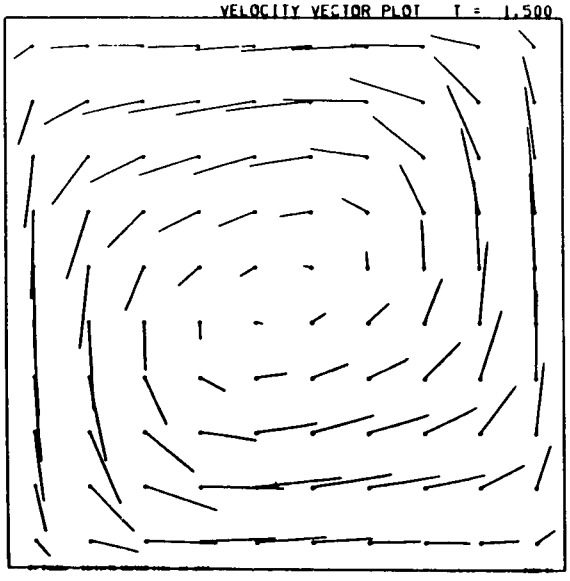

d. Steady State

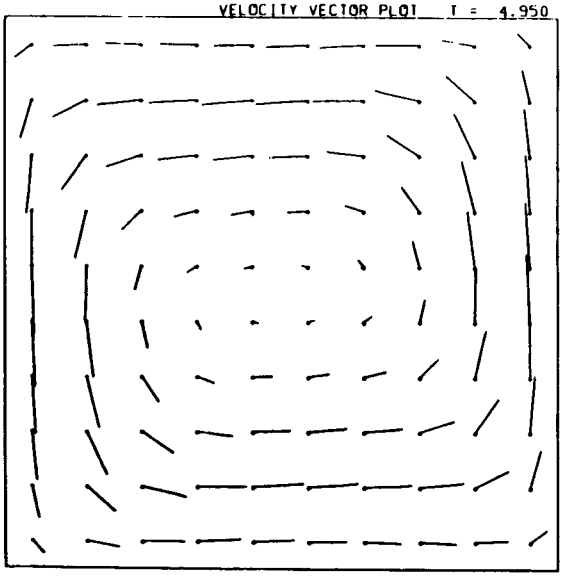

Figure 6 Comparison With Wilkes and Churchill

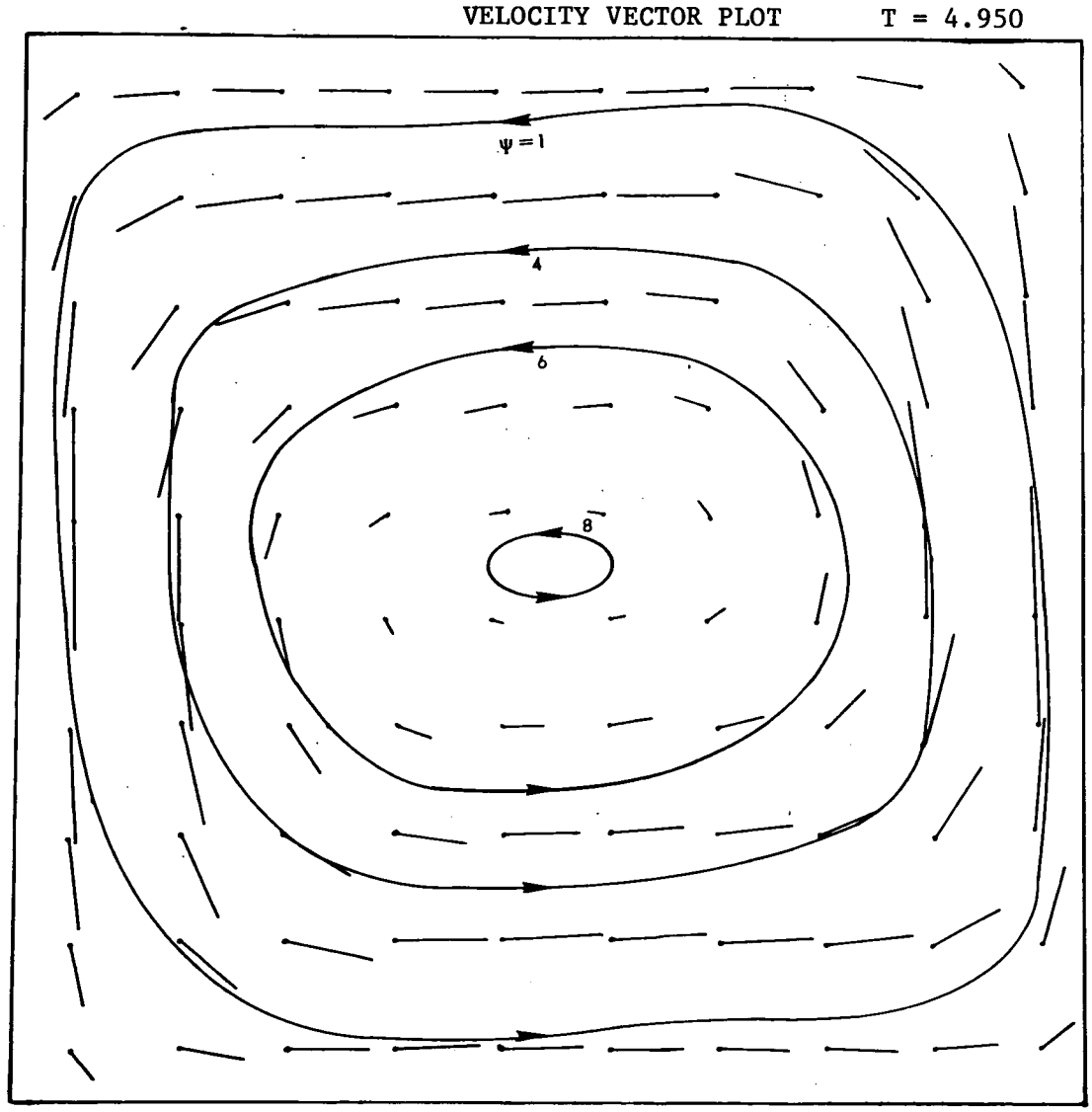

Figure 7 Steady-State Temperature Profiles

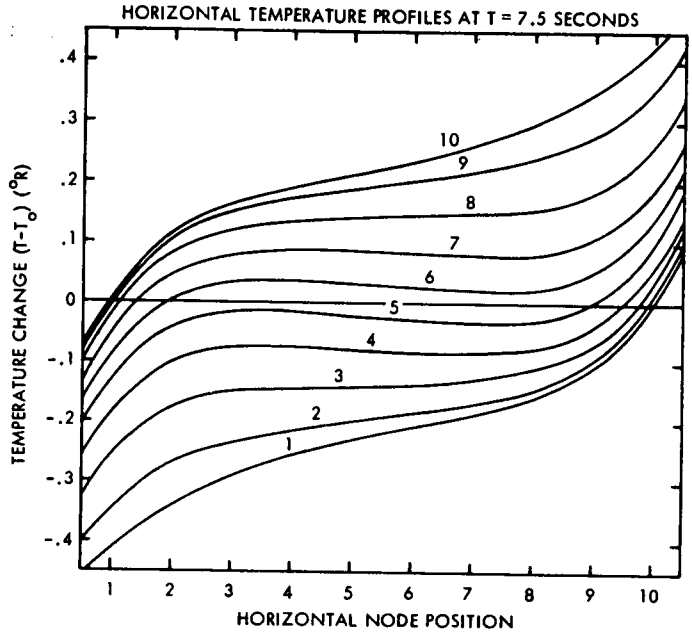

Figure 8 Steady-State Isotherms

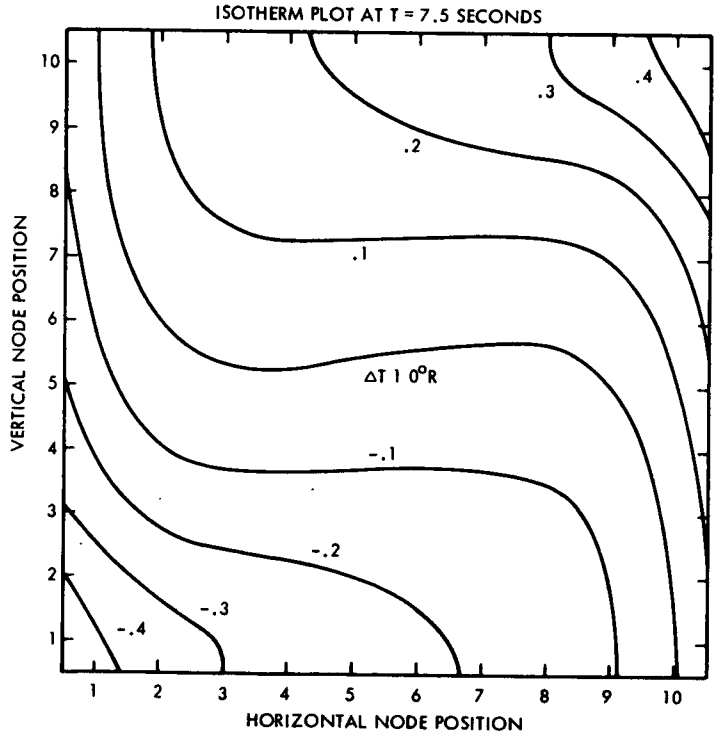

Figure 9 Apollo 12 Simulation Conditions

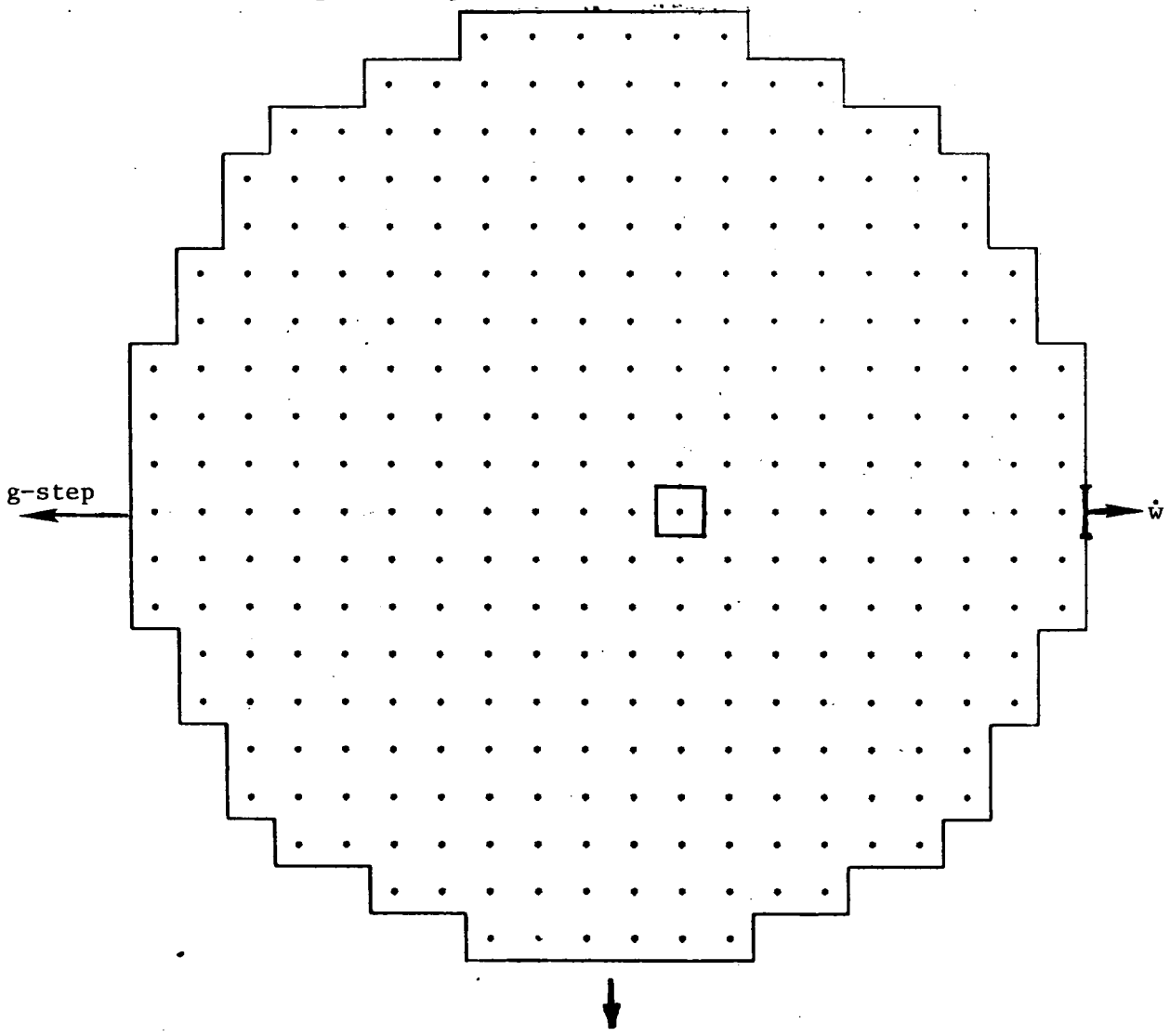

Conditions

P_o = 867.7 psi	Heater = 1 node
T_o = 200 °R	$\dot{q}$ = 528.6x(1/17) B/hr
ρ_o = 65.45 lbm/ft^3	$\dot{w}$ = 1.4x(3/40) lbm/hr
a = -2. x 10^{-8} G 's	Scale = 2400

Figure 10 Apollo 12 Stratified and Equilibrium Pressures

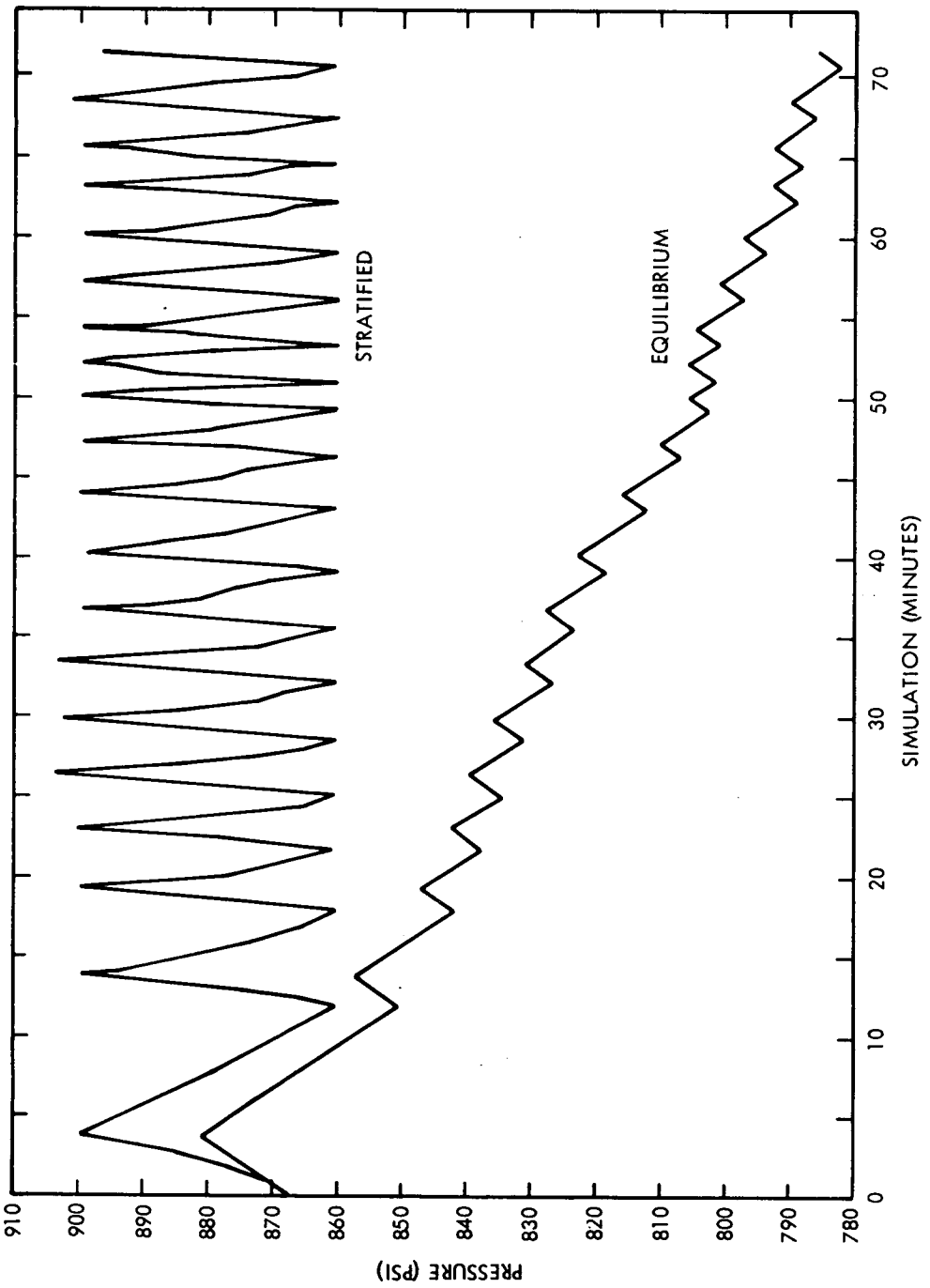

Figure 11 Apollo 12 Pressure Collapse

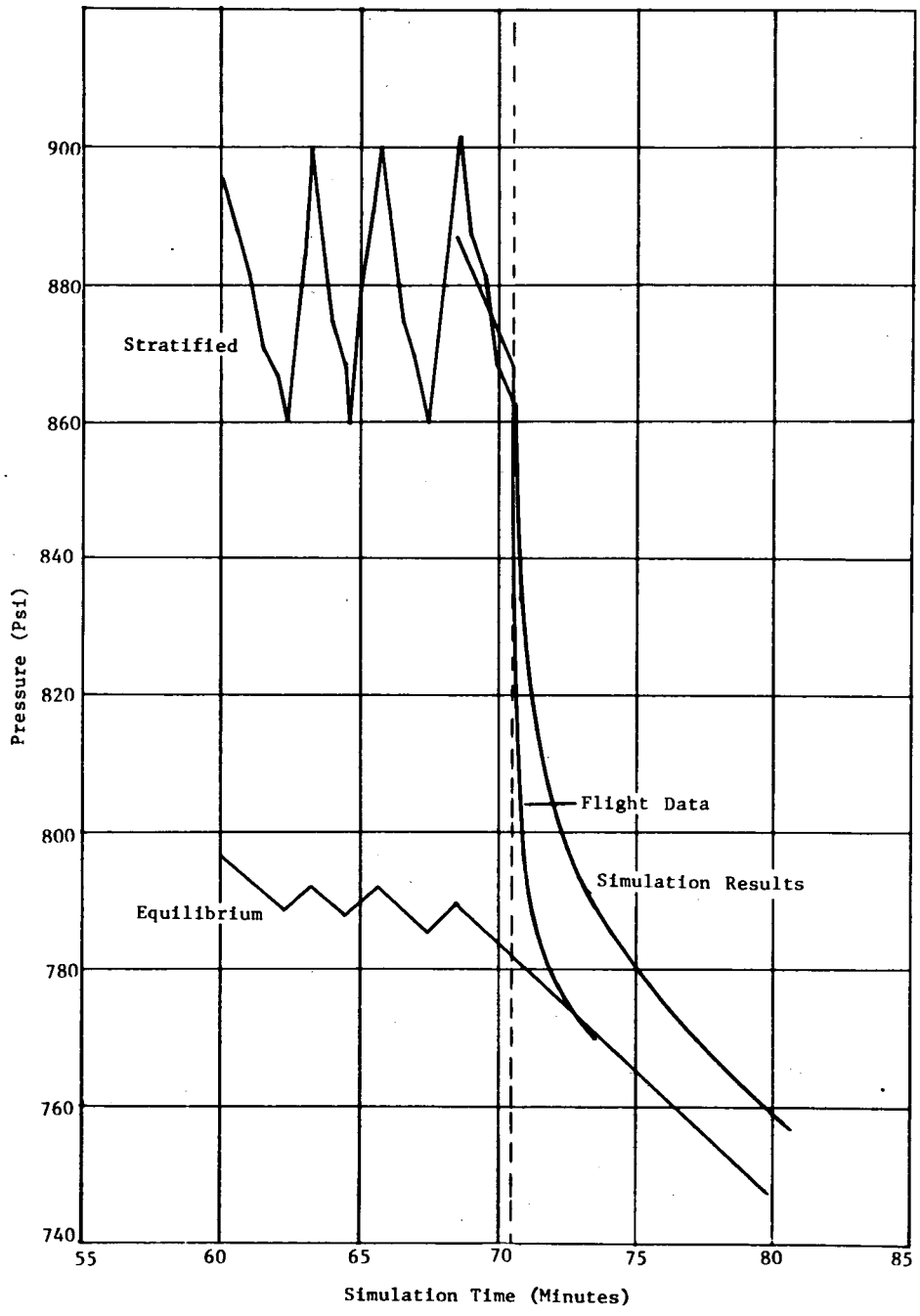

Figure 12 Apollo 12 Stratified Pressure - Including Refinements

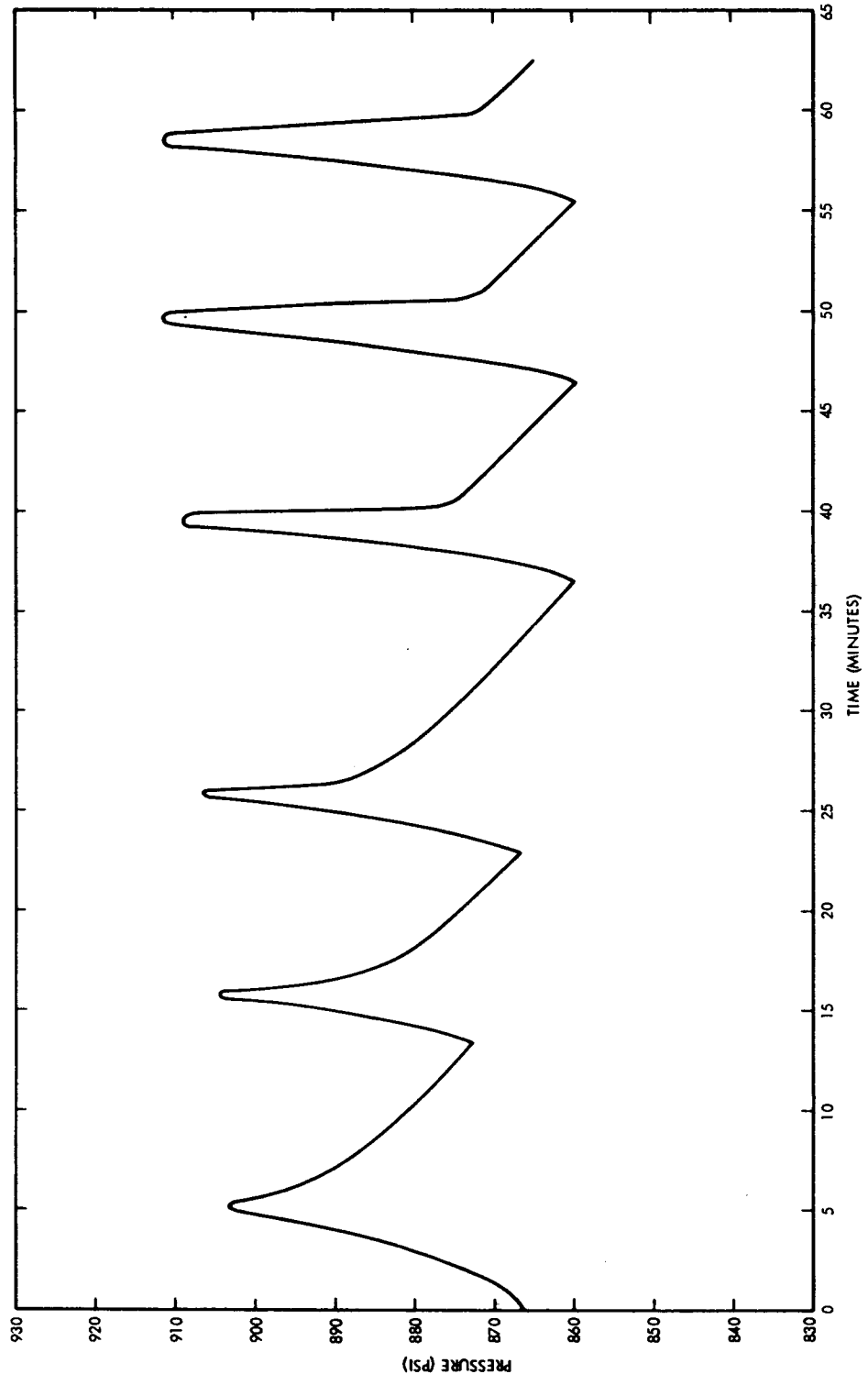

Figure 13 Apollo Convection at 2×10^{-5} G's

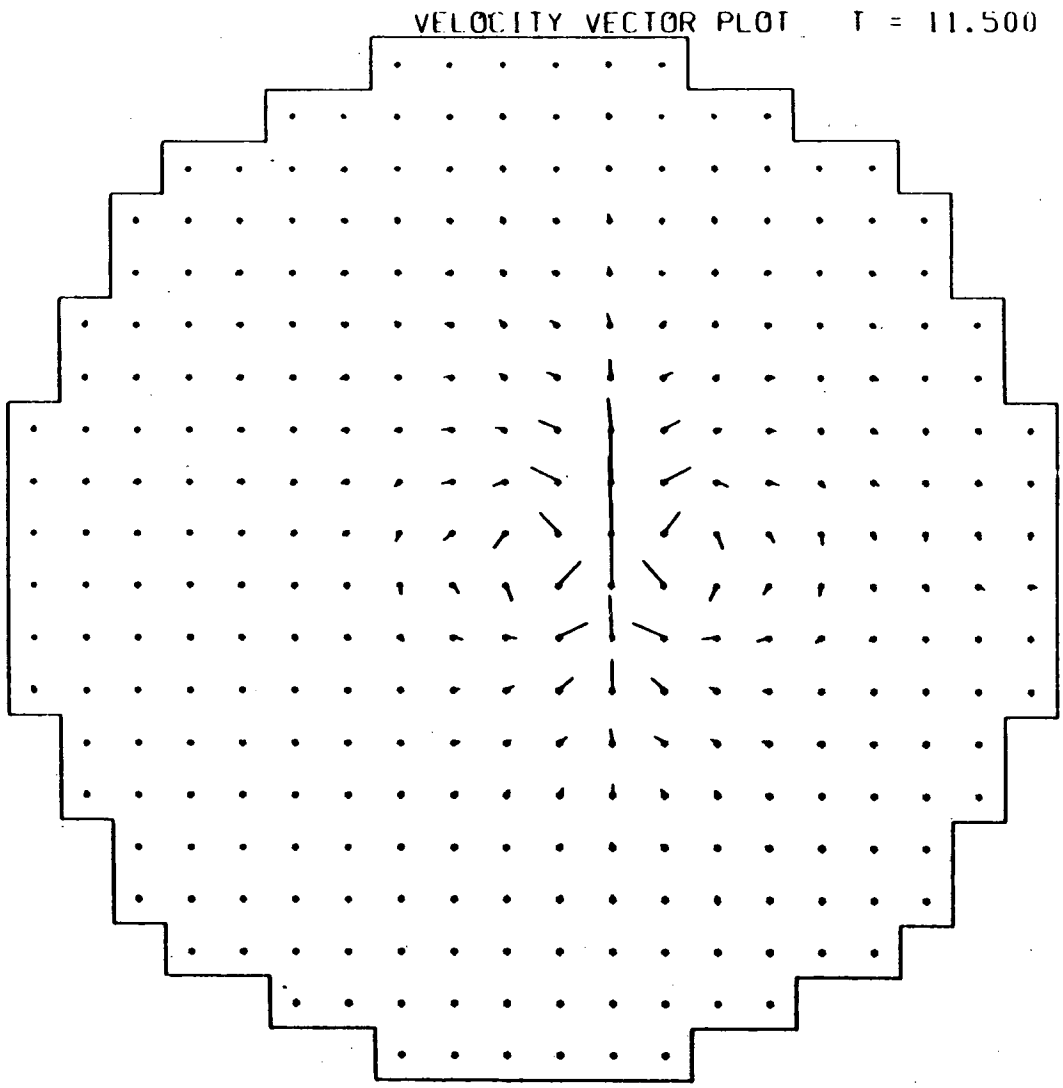

Figure 14 Surface Effects Under High Boundary Heat

a.

Test Conditions

P_o = 850 psi

T_o = 200 °R

L = .1 ft

g_y = -2 x 10^{-5} G's

$\dot{Q}_{leak}$ = 2000 B/hr

dV/dP = 0

$\dot{Q}_{heater}$ = 0

$\dot{W}_{outlet}$ = 0

Scale = 4800

Δt = .25 x 10^{-4}

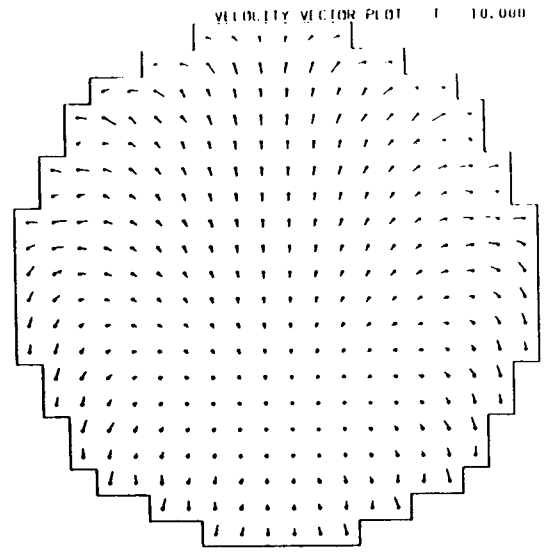

b.

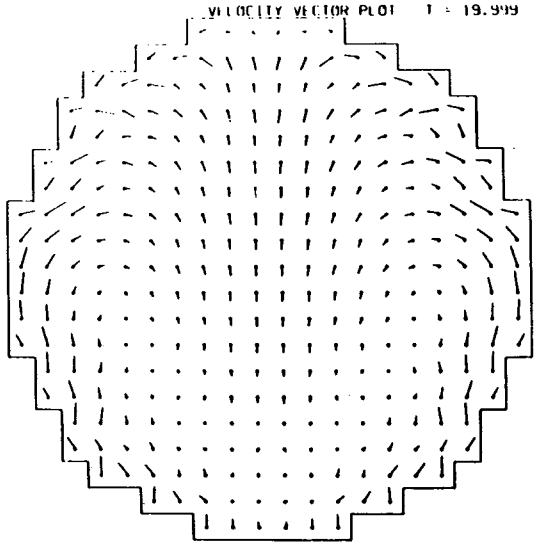

c.

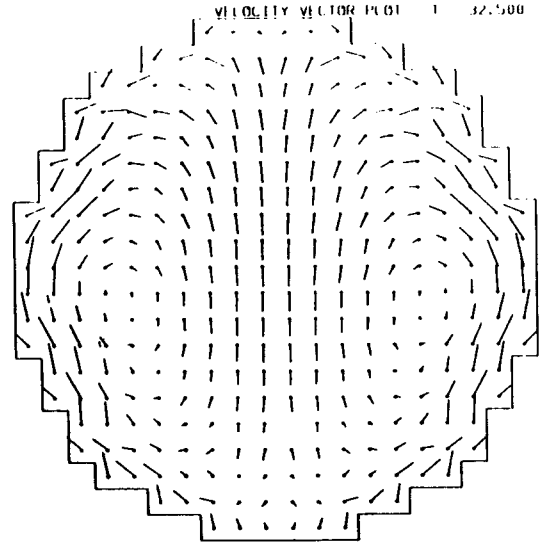

REFERENCES

1. Owens, S., "Apollo Fuel Cell and Cryogenic Gas Storage System Flight Support Handbook," NASA, MSC.

2. Kamat, D. V. and Abraham, W. H., "Pressure Collapse in Oxygen Storage Under Zero-g," Journal of Spacecraft & Rockets, Vol 5, No 2, Feb, 1968, ppg. 184-188.

3. Seto, R. K. M., et al, "Apollo Cryogenic Systems Programs," TRW Project Technical Report 17618-H090-R0-00, December 1970.

4. Richtmyer, R. D. and Morton, K. W., Difference Methods for Initial Value Problems, Interscience, New York, 2nd ed., 1967.

5. Schlichting, H., Boundary Layer Theory, McGraw-Hill, New York, 4th Ed., 1960.

6. Liepmann, H. W., and Roshko, A., Elements of Gasdynamics, Wiley, New York, 1957.

7. Goodrich, W. D., "A Numerical Solution for Problems in Laminar Gas Dynamics," PhD Dissertation, University of Texas at Austin, May, 1969.

8. Weber, L. A., "Thermodynamic and Related Properties of Oxygen from the Triple Point to 300 K at Pressures to 330 Atmospheres Supplement A (British Units)," National Bureau of Standards Report 9710 A, August 29, 1968.

9. Stewart, R. B., "The Thermodynamic Properties of Oxygen," PhD Thesis, University of Iowa, June 1966.

10. Chu, C. K., Editor, "Computational Fluid Dynamics," AIAA Selected Reprint Series, Vol 4, July 1968.

11. Ralston, A., and Wilf, H. S., Mathematical Methods for Digital Computers, Wiley, Vol. 1, 1960.

12. Cheng, S. I., "Numerical Integration of Navier-Stokes Equations," AIAA Journal, Vol. 8, No. 12, December 1970.

13. Rusanov, V. V., "The Calculation of the Interaction of Non-Stationary Shock Waves and Obstacles", National Research Council of Canada Library, Ottawa, Canada, Tech. Translation by D. A. Sinclair, 1962. Translated from: Zhurnal Vychislitelnoi Fiziki, Akademiya Nauk, SSSR 1, Vol. 1, No. 2, 1961, pp. 267 - 279.

14. Goodrich, W. D., Personal Communication, March 1971.

15. Heinmiller, P. J., "A Numerical Solution For The Prediction of Pressure Collapse in Supercritical Oxygen," TRW Project Technical Report 17618-H080-R0-00, December, 1970.

16. Roache, P. J., and Mueller, T. J., "Numerical Solutions of Compressible and Incompressible Laminar Separated Flows," AIAA Paper No. 68-741.

17. Wilkes, O. J. and Churchill, S. W., "The Finite-Difference Computation of Natural Convection in a Rectangular Enclosure," AIChE Journal, Vol. 12, No. 1, January 1966.

18. Slotnick, D. L., "The Fastest Computer," Scientific American Vol. 224, No. 2, February 1971.